Earth-Science Reviews 192 (2019) 355–378

Contents lists available at ScienceDirect

Earth-Science Reviews

journal homepage: www.elsevier.com/locate/earscirev

Intraplate magmatism at a convergent plate boundary: The case of the Cenozoic northern Adria magmatism

Valentina Brombin[a], Costanza Bonadiman[a,*], Fred Jourdan[b], Guido Roghi[c], Massimo Coltorti[a], Laura E. Webb[d], Sara Callegaro[e], Giuliano Bellieni[f], Giampaolo De Vecchi[f], Roberto Sedea[f], Andrea Marzoli[c,f]

[a] Dipartimento di Fisica e Scienze della Terra, Università di Ferrara, Italy
[b] Western Australian Argon Isotope Facility, School of Earth and Planetary Sciences, JdL Centre, Curtin University, Perth, WA, Australia
[c] Istituto di Geoscienze e Georisorse, CNR, Padova, Italy
[d] Department of Geology, University of Vermont, VT, USA
[e] Centre for Earth Evolution and Dynamics, University of Oslo, Norway
[f] Dipartimento di Geoscienze, Università di Padova, Italy

ARTICLE INFO

Keywords:
Intraplate magmatism
$^{40}Ar/^{39}Ar$ geochronology
Poloidal mantle flow
Southeastern Alps
Veneto Volcanic Province

ABSTRACT

The complex European–Adria geodynamic framework, which led to the formation of the Alpine belt, is considered responsible for the orogenic magmatism that occurred in the Central Alps along the Periadriatic/Insubric Line (late Eocene–early Oligocene) and the anorogenic magmatism that occurred in the Southeastern Alps (late Paleocene–early Miocene). While the subduction-related magmatic activities are, as expected, near convergent margins, the occurrence of the intraplate-related magmatism is still puzzling. Therefore, in this work new geochemical and geochronological data of magmatic products from the Veneto Volcanic Province (VVP, north–east Italy) are provided to constrain the Cenozoic intraplate magmatism of the Southeastern Alps. The VVP is formed by dominant basic–ultrabasic (from nephelinites to tholeiites) magmatic products and by localized acid (latitic, trachytic, and rhyolitic) volcanic and subvolcanic bodies. Trace element patterns and ratios suggest that the mantle source of the alkaline magma types was a garnet lherzolite possibly metasomatised by carbonatitic melts and with residual phlogopite.

According to the biostratigraphic records and our new $^{40}Ar/^{39}Ar$ ages, VVP eruptions occurred in several pulses, reflecting the extensional phases experienced by the Eastern Alpine domain. The volcanism started in the late Paleocene in the western sector of the VVP where activity was widespread also during the Eocene (45.21 ± 0.11 Ma – 38.73 ± 0.44 Ma). In the eastern sector eruptions took place in the early Oligocene (32.35 ± 0.09 Ma – 32.09 ± 0.29 Ma) and in the early Miocene (~23–22 Ma).

From the studies so far undertaken, the anorogenic magmatic activity of the VVP was interpreted as resulting from mantle upwellings through slab window(s) following the European slab break-off, which occurred at ~ 35 Ma. However, considering (i) new tomographic images evidencing a continuous subvertical (~ 500 km in depth) slab beneath the Central Alps, and (ii) the onset of magmatic activity in the VVP in the late Paleocene (i.e., before the slab break-off) and its continuation until the Miocene, a better suited geodynamic scenario is required to explain the anorogenic magmatism. The westward rollback of the European slab caused the retreat and steepening of the subducting plate. As a consequence, sub-slab mantle material escaped and upwelled from the front of the slab and created a poloidal mantle flow. The latter induced the breakdown of carbonates in calcareous metasediments and carbonated metabasics within the subducting oceanic slab, providing carbonatitic melts, which could be responsible for the metasomatism of the VVP mantle sources. After that, the poloidal mantle flow also induced (i) the extensional deformation in the overriding Adria microplate, (ii) the decompressional melting of VVP mantle sources, and (iii) the intraplate affinity of the VVP magmatism. During these processes, the Adria microplate also rotated counterclockwise, forming sedimentary basins, and allowing the poloidal mantle flow to affect different portions of the overlying lithosphere, generating *syn*-estensional magmatism within the VVP.

* Corresponding author.
E-mail address: bdc@unife.it (C. Bonadiman).

https://doi.org/10.1016/j.earscirev.2019.03.016
Received 24 September 2018; Received in revised form 13 March 2019; Accepted 20 March 2019
Available online 22 March 2019
0012-8252/

1. Introduction

Synchronous orogenic (or subduction-related) and anorogenic (or intraplate-like) magmatic events can occur near subductive zones. Worldwide examples are represented by the Okete–Alexandra Volcanic Province in New Zealand (Briggs and McDonough, 1990; Cook et al., 2005; Faccini et al., 2018); northwest Turkey (Aldanmaz et al., 2006); the Perşani volcanic field and South Harghita, in the southeast Carpathians (Seghedi et al., 2011; Faccini et al., 2018); the Kurdistan Province, western Iran (Allen et al., 2013); the Jeju volcanic field in Korea (Brenna et al., 2015); the Trans–Mexican Volcanic Belt (Neumann et al., 2016; Gómez-Tuena et al., 2018); the Payenia Volcanic Province in Argentina (Pallares et al., 2016). Calc-alkaline volcanism is expected at convergent margins (e.g., Fytikas et al., 1984; de Boer et al., 1988; Bradley et al., 2003; Kay et al., 2007; Aragón et al., 2013; Gómez-Tuena et al., 2018), whereas many interpretations have been proposed to explain the apparently unusual occurrence of magmatism with intraplate geochemical signatures in collisional settings. These magmas have been related to (i) ongoing rifting with spreading-ridge jump beneath the continental crust (Luhr et al., 1985; Allan et al., 1991); (ii) upwelling of a mantle plume through a slab window after a slab detachment (e.g., Davies and von Blanckenburg, 1995; von Blanckenburg and Davies, 1995; Ferrari, 2004); (iii) activation of extensional faulting in the foreland after a collisional event (e.g., Verma, 2002; Aldanmaz et al., 2006); (iv) formation of a mantle corner flow which upwells from the rear arc to the top of the slab and then descends along the sinking slab (Gómez-Tuena et al., 2018); and (v) lateral and frontal inflow of the asthenospheric mantle into the mantle wedge region induced by sinking and rollback of the slab (e.g., Ferrari et al., 2001; Coltorti et al., 2009; Faccenna et al., 2011; Neumann et al., 2016). The geodynamics of subduction processes is still matter of ongoing research (e.g., Dal Zilio et al., 2018), it is not surprising that the petrological community proposed so many geodynamic models, some of them in contrast with each other, to explain the occurrence of intraplate-like magmatism near convergent margins. Therefore, in order to contribute to this (global scale) debate we investigated the relationship between the Alpine regional tectonic evolution and the alkaline to tholeiitic magmatic activity that affected the Southeastern Alps from the Paleocene to the Miocene. Despite the history of the Alpine belt is considered as a classical geological case study to investigate the formation and evolution of the collisional orogens, its related intraplate magmatism is still poorly studied. Such magmatic activity generated the Veneto Volcanic Province (VVP), one of the largest magmatic districts of the Adria microplate (Fig. 1). The VVP magmas have an intraplate geochemical signature. Nonetheless, they are almost coeval with the middle Eocene–early Oligocene sub-alkaline to calc-alkaline basic plutons and dikes intruded along to the Periadriatic/Insubric Line in the Central Alps displaying a calc-alkaline, subduction-related fingerprint (i.e., Bergell, Triangia, Adamello; Fig. 1a). Given the large interest in the geodynamic processes that generated the Alpine chain, the subduction-related magmatism of the Central Alps was examined by numerous petrological, geochemical, and geochronological studies (Brack, 1981, 1984; Kagami et al., 1991; von Blanckenburg, 1992; Callegari and Brack, 2002; Oberli et al., 2004; Harangi et al., 2006; Conticelli et al., 2009; Schaltegger et al., 2009, 2019; Alagna et al., 2010; Bellieni et al., 2010; Bergomi et al., 2015). The Periadriatic Cenozoic magmatism is generally related to upwelling of asthenospheric mantle material through a slab window, which formed after the late Eocene Adria–Europe continental collision (~35 Ma; Stampfli et al., 1998, 2002; Rosenbaum and Lister, 2005). The mantle flow heated the supra-subduction hydrated mantle wedge, causing melting of the Adria subcontinental lithosphere (Bergomi et al., 2015). According to some authors (e.g., Macera et al., 2003; Bergomi et al., 2015), the slab break-off occurrence may explain also the alkaline magmatism in the Southeastern Alps: mantle diapirs were sucked into the slab window and upwelled towards shallower levels heating the overriding lithospheric plate to the point of triggering partial melting. Recently, Niu (2017) and Garzanti et al. (2018) evidenced the abuse of invoking the slab break-off process by the geological community even when the “evidences” (e.g., tomographic images) are not well constained or are contradictory. The slab break-off process was proposed for the first time by Davies and von Blanckenburg (1995) and von Blanckenburg and Davies (1995) to explain the onset of Periadriatic magmatism and the initial exhumation of high-pressure rocks along the Alps. Since those pioneering studies, the slab break-off mechanism was invoked to explain a range of phenomena occurring near convergent margins, including: (i) exhumation of metamorphic rocks (e.g., eclogites in the Himalaya; O'Brien, 2001); (ii) topographic uplift (e.g., in the Appennines, Italy; Carminati et al., 1998); (iii) ore mineralization (e.g., gold mineralization in the Jiaodong Peninsula, China; Yang and Santosh, 2014); (iv) inversion of subduction polarity (e.g., switch of the Alpine subduction polarity from SE to NW-dipping; Handy et al., 2010); and (v) intraplate magmatism (e.g., VVP in the Eastern Alps; Macera et al., 2003). The most important evidence supporting the slab break-off hypothesis comes from seismic tomographic studies showing “low-velocity anomalies” interpreted as slab gaps. However, Foulger et al. (2015) demonstrated fundamental limitations and uncertainties of the seismic tomographic models in the quantification of the observed anomalies.

In this scenario, a detailed knowledge of the age of emplacement of the magmatic products as well as of their main geochemical features is crucial for the understanding of the geodynamic significance of the VVP. Aiming to unravel the link between the Alpine orogenesis and the VVP magmatism and to constrain the potential nature and evolution of the mantle source(s) of this magmatism, we review the previously published geochemical data and geochronological data (including radioisotopic and biostratigraphic constraints) and combine them with new geochemical data and $^{40}Ar/^{39}Ar$ ages of magmatic products from the VVP.

2. A brief description of geological evolution of the Alps

Both orogenic and anorogenic igneous activities within the Alpine realm are connected with the relative movements of the European plate and Adria microplate, which are still debated. Convergence of these two plates is considered to have started in the Early Cretaceous as a result of the final closure of the Meliata Ocean, a back-arc basin, which separated the two continental segments since the early Permian (Stampfli et al., 1998, 2002; Rosenbaum et al., 2002; Dézes et al., 2004; Schmid et al., 2004; Rosenbaum and Lister, 2005). The convergence of the Adria microplate and the European plate marks the onset of the Alpine orogenesis along the northern margin of Adria (Stampfli et al., 1998, 2002; Rosenbaum et al., 2002; Schmid et al., 2004; Rosenbaum and Lister, 2005). In particular, orogenic processes took place first in the Eastern Alps (peak of high-pressure metamorphism at ~100–90 Ma) and then in the Western Alps (peak of high-pressure metamorphism at ~85–60 Ma) (Manzotti et al., 2014, and references therein). During the Paleocene (at ~65–55 Ma), convergence ceased for a period of 10 My due to Adria–Europe continental collision in the Eastern Alps after the subduction of the easternmost portion of Piedmont–Liguria Ocean beneath the advancing orogenic wedge (Stampfli et al., 1998, 2002; Rosenbaum et al., 2002; Dézes et al., 2004; Schmid et al., 2004; Rosenbaum and Lister, 2005). Since the early Eocene the reprise of the Adria–Europe convergence led to the subduction and final closure of the Piedmont–Liguria Ocean and Valais Ocean in the Western Alps domain at ~45 Ma and ~35 Ma, respectively (Rubatto et al., 1998; Stampfli et al., 1998, 2002; Rosenbaum and Lister, 2005). According to numerous studies, the subducted oceanic lithospheric slab of the Central and Eastern Alps detached from the European foreland lithosphere after closure of the Valais Ocean (e.g., Davies and von Blanckenburg, 1995; von Blanckenburg and Davies, 1995; Stampfli et al., 1998, 2002; Dézes et al., 2004). During the Eocene with the ongoing Adria–Europe

collision, E–W extension developed parallel to the orogenic belt in the Eastern Alps (Ratschbacher et al., 1989; Zampieri, 1995). From the Oligocene (~34 to ~28 Ma), such rifring phase affected also the Central Alps (Ring, 1994; Nievergelt et al., 1996; Challandes et al., 2003; Glodny et al., 2008; Pleuger et al., 2008; Steck, 2008; Beltrando et al., 2010; Ring and Gerdens, 2016; Schmid et al., 2017). This extensional phase of the overriding plate was probably induced by the rollback of the retreating SE–dipping slab (Rosenbaum and Lister, 2005). From

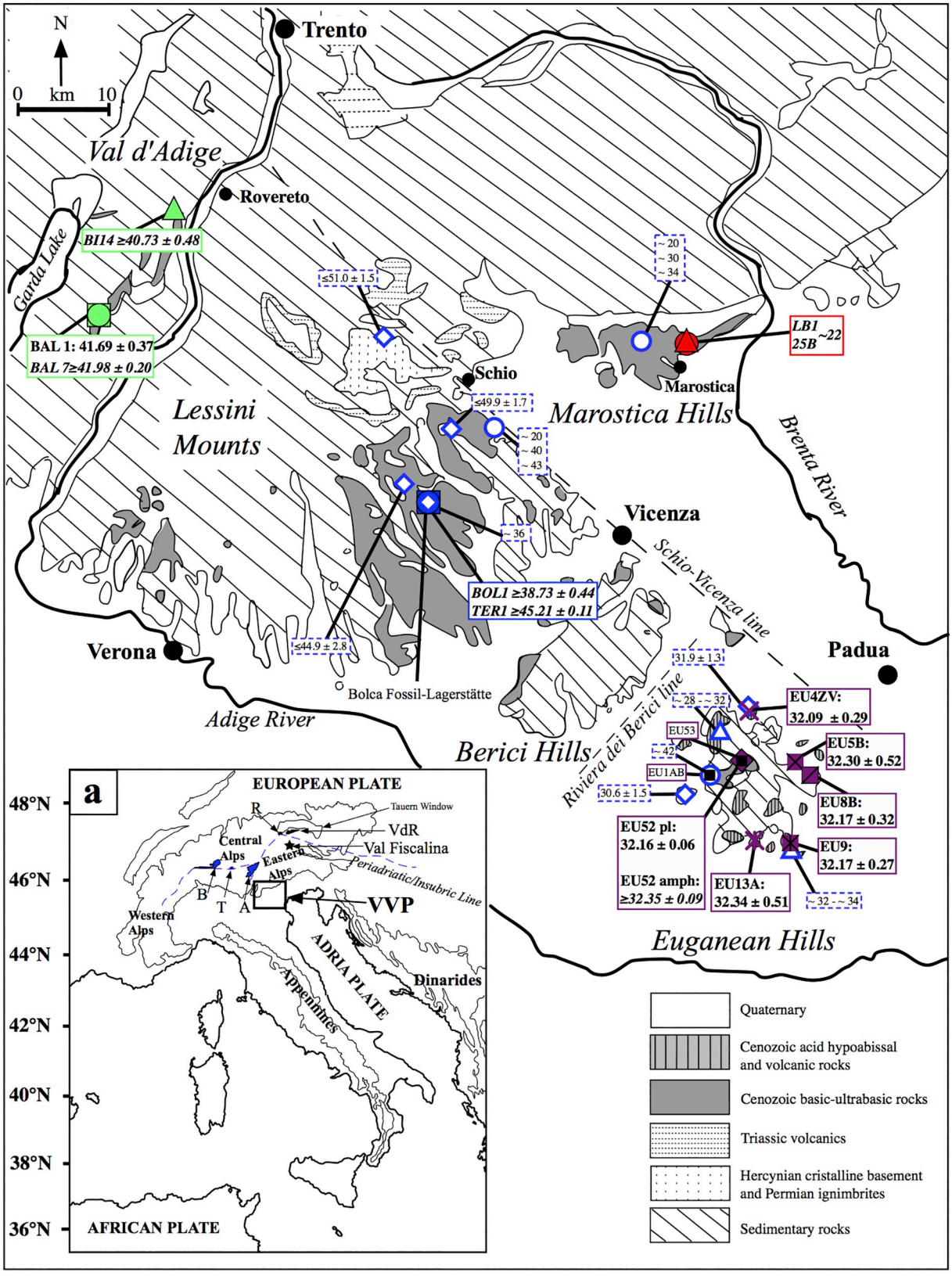

(caption on next page)

Fig. 1. Simplified geological map of the Veneto Volcanic Province (VVP; De Vecchi and Sedea, 1995), showing the locations of the samples collected for this work. Ages and uncertainties (in Ma) of the magmatic rocks occuring in the VVP are framed with continuous line ($^{40}Ar/^{39}Ar$ ages of this work) and dashed line (literature data). Ages in italics are derived from mini-plateaus (50–70% ^{39}Ar released) and are considered minimum ages (see explanation in Section 9, and in section S2 of the Supplementary materials).
Black squares are samples of this work for which $^{40}Ar/^{39}Ar$ analysis was not performed; open blue diamonds are U–Pb ages (Visonà et al., 2007; Bartoli et al., 2014); open blue triangles are Rb–Sr ages (Zantendeschi, 1994); open blue circles are K–Ar dates (Borsi et al., 1969; Savelli and Lipparini, 1979).
Inset (a) present-day location of VVP in the Italian peninsula, in relation to European and African plates and Adria microplate (modified from Carminati and Doglioni, 2012) and locations of Periadriatic basic (blue patterns) and acid (black patterns) plutons along the Periadriatic/Insubric line. Abbreviation for plutons: B = Bergell, T = Trigia, A = Adamello, R = Rensen, VdR = Vedrette di Ries. (For interpretation of the references to color in this figure legend, the reader is referred to the web version of this article.)

~30 Ma until the Oligocene–Miocene boundary (~23 Ma), the extensional processes stopped and large-scale coarse clastic sedimentation occurred in the Eastern Alps in response to an accretionary event (Frisch et al., 2000; Rosenbaum and Lister, 2005). Another phase of extension occurred during the early and middle Miocene due to the onset of lateral tectonic extrusion, which rearranged the structural pattern and created the present elongated shape of the Eastern Alps (Ratschbacher et al., 1991; Frisch et al., 2000). This lateral tectonic extrusion is ascribed to a combination of gravity-driven orogenic collapse because of an over-thickened lithosphere, and to a tectonic escape along conjugate fault zones driven by tangential forces due to continuing N–S convergence between the Adria microplate and the European plate (Ratschbacher et al., 1991; Frisch et al., 2000). However, the amount of Oligocene extension was limited, focused in the eastern Tauern Window (Fig. 1a) and to the east of it, whereas Miocene extension occurred at a larger scale (Ratschbacher et al., 1991).

3. The Cenozoic Central and Southeastern Alpine magmatism

Cenozoic magmatism within the Alpine realm is variable in time and space reflecting the changing geodynamic framework during the convergence of the Adria microplate and the European plate (Bassi et al., 2008). In the Central Alps, the magmatic activity was orogenic and essentialy intrusive along the Periadriatic/Insubric line (Fig. 1a), represented by sub-alkaline and calc-alkaline basic to acid intrusive bodies and basaltic and andesitic dikes with calc-alkaline to shoshonitic affinity. Based on radioisotopic ages, the climax of such magmatism ranged from ~34 to ~28 Ma (von Blanckenburg and Davies, 1995; Rosenberg, 2004). However, the first evidence of igneous activity dates back at ~43 Ma with the emplacement of the southern Adamello batholith and coeval dikes (Schaltegger et al., 2009, 2019; Schoene et al., 2012; Bergomi et al., 2015). On the contrary, in the Southeastern Alps the magmatic activity was effusive to subvolcanic with magmas yielding an anorogenic geochemical signature (Beccaluva et al., 2007). This magmatism occurred in a NNW–SSE elongated area of about 1500 km^2, defining from northwest to southeast five main volcanic districts: Val d'Adige, Lessini Mts., Marosticano, Berici Hills, and Euganean Hills (Beccaluva et al., 2007). Together, these districts constituted a Cenozoic magmatic province in the Southeastern alpine domain known in literature as Veneto Volcanic Province (VVP; e.g., De Vecchi and Sedea, 1995; Beccaluva et al., 2001, 2007; Macera et al., 2003, 2008; Visonà et al., 2007) (Fig. 1a).

3.1. Is the VVP part of a wider European anorogenic Cenozoic magmatism?

Cenozoic anorogenic magmatic activity was not limited to the VVP area. From the early Cenozoic to recent times anorogenic magmatism was widespreaded around the central-western Mediterranean and in central-western Europe (Wilson and Downes, 2006; Lustrino and Wilson, 2007, and references therein). Lustrino and Wilson (2007) referred to this widespread activity as the CiMACI (Circum-Mediterranean Anorogenic Cenozoic Igneous) province. The European magmatic activity started in the Paleocene–Eocene in the VVP, in the French Massif Central, in the Bohemian Massif, in the eastern Serbia, and in the Pannonian Basin (Hungary) (Wilson and Downes, 2006). During the Oligocene–Miocene, the volcanic phases were recorded in even more areas (in the VVP, in the Eger-Ohre Graben in Czech Republic; in the Rhenish Massif and the Rhine Graben in Germany; in the Massif Central in France; in the Styrian Basin in Austria; in the Pannonian Basin; in the Calatrava province in Spain; in Sicily; Wilson and Downes, 2006). This magmatism was contemporaneous with the development of an extensive intracontinental rift system (the East and Central European Rift System, ECRIS), linked to the collision of Africa and Eurasia plates (Wilson and Downes, 1992; Dézes et al., 2004). Several geodynamic models were proposed to explain the origin of the European Cenozoic anorogenic magmatic districts: (i) a mantle plume upwelling from the core-mantle boundary (e.g., Goes et al., 1999; Wedepohl and Baumann, 1999); (ii) a mantle plume, whose tail was anchored beneath the Cape Verde-Madeira-Canary Islands region, and whose large head was dragged by the movement of Eurasia towards the northeast, where local extensional tectonics and slab ruptures triggered plume-related volcanism (Macera et al., 2003); (iii) multiple mantle plumes upwelling from a single upper mantle reservoir located in the Transition Zone (Wilson and Patterson, 2001). The similar Sr-Nd-Pb isotopic signatures of the magmatic products (including those of the VVP) point to a common sub-lithospheric mantle reservoir from western Europe to the Mediterranean area. This common mantle reservoir is called European Asthenospheric Reservoir (EAR; Hoernle et al., 1995; Wilson and Downes, 1991, 2006), or Prevalent Mantle (PreMa; Wörner et al., 1986), or Common Mantle Reservoir (CMR; Lustrino and Wilson, 2007). Deviations and compositional variations from the mantle reservoir composition are commonly explained as the result of mixing of EAR-derived melts with heterogeneous lithospheric mantle sources originated from earlier silicate/carbonate melts or metasomatic fluids, which could be related to subduction processes (Pfänder et al., 2018). For example, in case of the VVP, according to Beccaluva et al. (2007) the most alkaline magmas, which were generated from the deepest mantle sources, show a relatively stronger HIMU signature. Conversely, the sub-alkaline magmas, which were generated at shallower depths in the lithospheric mantle, record a slight EMII signature. In particular Macera et al. (2003) proposed a pelagic sediment contribution for the crustal component, which affected the Lessini basanites and a terrigenous sediment contribution to the source of the Euganean transitional basalts.

3.2. Geological outline of the VVP

Magmatic activity started in the VVP already in the Paleocene (Bassi et al., 2008), along the Jurassic Trento carbonate platform, which encompassed the Val d'Adige and the Lessini Mts. areas (Winterer and Bosellini, 1981; Dewey et al., 1989; Zampieri, 1995). After the Adria–Europe collision in the Eastern Alps (~65 Ma; Stampfli et al., 1998, 2002; Rosenbaum et al., 2002; Dézes et al., 2004; Schmid et al., 2004; Rosenbaum and Lister, 2005), extension developed (Ratschbacher et al., 1989). As a consequence, in the Southeastern Alpine domain the rigid Trento platform block-faulted forming a horst and graben structure, called the Alpone–Agno Graben (Zampieri, 1995). Until the middle Eocene the extensional tectonics of the new NNW–SSE transtensional fault systems and the Alpone–Agno Graben controlled the deposition of limestone and the volcanic activity, which manifested

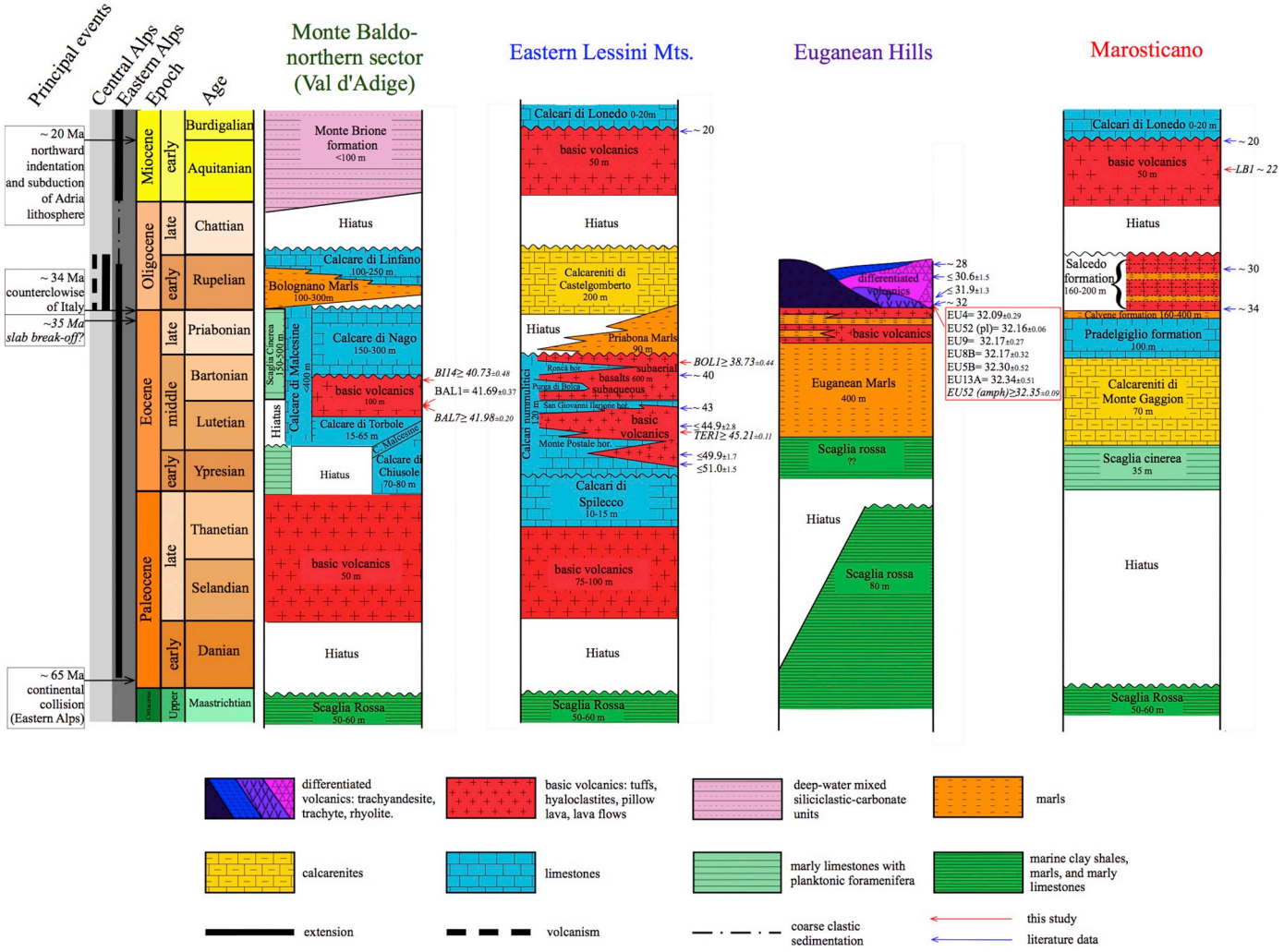

Fig. 2. Simplified Upper Cretaceous to lower Miocene stratigraphy of the studied areas: Monte Baldo northern sector (Val d'Adige district; Luciani, 1989; De Vecchi and Sedea, 1995), Eastern Lessini Mts. (De Vecchi and Sedea, 1995; Bassi et al., 2008), Euganean Hills (Piccoli et al., 1976, 1981), and Marosticano (Frascari Ritondale Spano and Bassani, 1973; De Vecchi and Sedea, 1995; Bassi et al., 2008). Ages and uncertainties are reported in Ma. Ages in italics are derived from mini-plateaus (50–70% ^{39}Ar released) and are considered minimum ages (see explanation in Section 9 and in the section S2 of the Supplementary materials). Ages derived from zircon analysis for the Lessini Mts. and the Euganean Hills districts are considered maximum ages (see explanation in Section 4). Previously published geochronological data are from Borsi et al. (1969), Savelli and Lipparini (1979), and Visonà et al. (2007) for the eastern Lessini Mts., from Borsi et al. (1969), Zantendeschi (1994), and Bartoli et al. (2014) for the Euganean Hills, and from Savelli and Lipparini (1979) for the Marosticano. The main geodynamic events, extension phases, and coarse clastic sedimentation occurred in Central and Eastern Alps are reported, as well as the climax of the orogenic Periadriatic Central Alps magmatism.

with short-lived pulses (Barbieri et al., 1991) in the Monte Baldo area of the Val d'Adige district and along the Lessini Mts. district (Luciani, 1989). Therefore, in the troughs of the horst and graben structure basic–ultrabasic hyaloclastites, volcanoclastics, subaqueous, and subaerial lava flows were accumulated and interbedded between the Scaglia Rossa (Upper Cretaceous–late Paleocene) and the Eocene limestones, or within the latter (Fig. 2).

According to biostratigraphic data the magmatic activity occurred later in the eastern VVP districts (i.e., the Euganean Hills and the Marosticano areas; Piccoli et al., 1976, 1981; Savelli and Lipparini, 1979; Luciani, 1989). From the late Eocene to the early Oligocene basic volcanic products were interbedded with marls of the Euganean Hills pelagic environment (De Vecchi et al., 1976; Piccoli et al., 1976, 1981; Fig. 2). In the early Oligocene, the Euganean magmatism changed and was dominated by rhyolites, trachytes and subordinately by trachyandesites (latites) and basalts, which formed mainly subvolcanic bodies and less abundant lava flows (De Vecchi et al., 1976; Piccoli et al., 1976, 1981). In the middle Oligocene, the magmatic activity resumed in the Marosticano (Fig. 2) and the Lessini Mts. districts in a subaqueous environment as testified by the marine sediments (sandstones, calcarenites, and limestones; Gavioli, 1972; Savelli and Lipparini, 1979) interbedded with the volcanic deposits (Fig. 2). Sparse Oligocene explosive and effusive volcanic activity is documented also in the Berici Hills (west of the Euganean Hills; Bassi et al., 2008). At the end of the late Oligocene, the Marosticano and the Lessini Mts. areas emerged (Frascari Ritondale Spano and Bassani, 1973) shortly before eruption of the last subaerial volcanic products at the beginning of the Miocene (Savelli and Lipparini, 1979). These volcanic deposits of these districts are overlain by coralline calcarenites of the early Miocene age (Frascari Ritondale Spano, 1969; Savelli and Lipparini, 1979; Fig. 2), testifying to a new transgression event.

4. Previous geochronological studies of VVP

The integration of stratigraphic records with reliable radioisotopic ages allows to (i) better constrain the distribution and the timeframe of such highly variable, but temporally short, magmatic activity and (ii) infer the geodynamic evolution of this magmatic province. Previously

obtained geochronological data are mainly K–Ar ages on basic–ultrabasic whole-rocks (Borsi et al., 1969; Savelli and Lipparini, 1979; Fig. 1). These K–Ar data suggested eruption ages of 42.5 ± 1.5 to 20.4 ± 0.8 Ma for the Lessini Mts., 42.0 ± 1.5 Ma for the Euganean Hills, and from 33.7 ± 1.2 to 20.4 ± 0.8 Ma for the Marosticano district. However, the reliability of such ages is questionable, as the K–Ar dating technique is not able to recognise (and correct for) non-atmospheric $^{40}Ar/^{36}Ar$ ratios and alteration effects (Oostingh et al., 2017). Zantendeschi (1994) dated Euganean trachytes and rhyolites using the whole-rock Rb–Sr method (Fig. 1), the obtained eruption ages span from 34 ± 2 to 28 ± 1 Ma. These ages also must be treated with caution, as the ^{87}Rb decay constant is still poorly defined and Rb/Sr isotopic system is prone to secondary alteration (Begemann et al., 2001; Schmitz et al., 2003). The most recent available radioisotopic data (Fig. 1) are U–Pb ages obtained using a sensitive high-resolution ion microprobe (SHRIMP) on zircons hosted (i) in a porphyritic basanite lava and in two altered dykes of the Lessini Mts. (Visonà et al., 2007) and (ii) in magmatic enclaves within trachytes of the Euganean Hills (Bartoli et al., 2014). These ages may be interpreted as maximum ages of eruptions as the analysed zircons were not crystallized directly from the erupted magma. The Lessini Mts. zircons yielded Eocene ages spanning from 51.1 ± 1.5 to 44.9 ± 2.8 Ma (Visonà et al., 2007), even if it should be considered that these data are not concordant. Zircons from the Euganean Hills xenoliths yielded Oligocenic ages of 31.9 ± 1.3 Ma and 30.6 ± 1.5 Ma (Bartoli et al., 2014).

From this overview on the currently available geochronological data and related uncertainties, it is clear that more accurate age data are essential for the temporal reconstruction of the VVP magmatism. In this work, new high-resolution ages were obtained using the $^{40}Ar/^{39}Ar$ systematic on groundmass samples and on mineral separates, which is currently widely accepted as an accurate dating technique (McDougall and Harrison, 1999).

5. Sampling

Following biostratigraphic information we selected our samples in order to encompass most of the time range of the VVP magmatism. From the Val d'Adige and the Lessini Mts., the two presumably oldest magmatic districts, samples were collected from basic–ultrabasic lava flows and volcanic necks. BAL1 and BAL7, two out of three samples from the Val d'Adige district, are from the northeastern part of Monte Baldo (Table 1; Fig. 1). BAL1 was collected nearly at the top of a subaqueous lava flow interbedded between middle and late Eocene limestones (Calcare di Torbole and Calcare di Nago; Fig. 2), whereas BAL7 was sampled from a thin sill between Cretaceous–Paleocene (Scaglia Rossa) and middle Eocene limestones (Calcare di Torbole; Fig. 2). The third sample from the Val d'Adige district, BI14, was collected from a volcanic neck exposed in a quarry near Rovereto (Table 1; Fig. 1). The sampling for the Lessini Mts. district was focused near the famous Bolca Fossil-Lagerstätte area (Papazzoni et al., 2014, and references therein; Fig. 1). Sample TER1 (Table 1; Fig. 1) was collected from a lava flow interbedded with red clays of unknown age, whereas sample BOL1 (Table 1; Fig. 1) was collected from the volcanic neck preserved near the mentioned fossiliferous area. This neck cuts 10–20 m of freshwater-brackish sediments of probable Ypresian age (Barbieri and Medizza, 1969; Medizza, 1980; Sorbini, 1989; Giusberti et al., 2014).

The Euganean Hills are the only VVP magmatic district where basic, intermediate, and acid magmas erupted or intruded at shallow-depth forming lava flows and subvolcanic bodies (mainly laccoliths) during the late Eocene–early Oligocene (Fig. 2). We have sampled and analysed rocks in order to investigate the entire range of lithologies. Samples EU1AB, EU53, EU52, EU8B, and EU13A represent the least differentiated products of the Euganean sample suite. The basaltic andesite lava flow EU1AB was collected from an outcrop in the western part of the Euganean Hills (Table 1; Fig. 1). The basaltic andesite sample EU53 was collected from a subvolcanic body at the center of the Euganean Hills, and the basaltic trachyandesite EU52 from an intrusion cutting this basaltic andesite body (Table 1; Fig. 1). The basaltic trachyandesite EU8B and the latite EU13A were collected from subvolcanic bodies (Monte Oliveto and Monte Cecilia), in the eastern and southern sectors of the Euganean Hills, respectively (Table 1; Fig. 1). Samples EU4, EU5B, and EU9 represent the acid products of the Euganean Hills. The trachyte EU4 (Monte Merlo quarry, northern sector of the Euganean Hills; Table 1; Fig. 1), the rhyolite EU5B (Monte Alto, eastern sector; Table 1; Fig. 1), and the rhyolite EU9 (Monte Ricco, southeastern sector; Table 1; Fig. 1), were collected from laccoliths intruded in the Euganean Marls Formation (Oligocene; Piccoli et al., 1976, 1981; Fig. 2).

Finally, for the Marosticano district, where probably the youngest VVP magmatic events occurred, we sampled two specimens (LB1 and 25B). These samples were collected from the ultrabasic volcanic neck cutting the middle Oligocene marine sediments of the Salcedo formation at Monte Gloso (Savelli and Lipparini, 1979; Table 1; Figs. 1 and 2).

6. Analytical methods

Whole-rock major and trace elements were determined by Wavelength Dispersive X-Ray Fluorescence Spectrometry (WDXRF) at the University of Ferrara (IT; ARL Advant-XP spectrometer) and at the University of Padova (IT; Philips PW1404). Rb, Sr, Y, Zr, Nb, Hf, Ta, Th, U, and rare-earth elements (REEs) were performed with Inductively Coupled Plasma–Mass Spectrometry (ICP-MS) at the University of Ferrara (Thermo Series X-I spectrometer) and at the University of Bretagne Occidentale, Brest (FR; Thermo Element2). Clinopyroxene compositions were determined by means of a CAMECA SX50 electron microprobe at the IGG-CNR of Padova.

For $^{40}Ar/^{39}Ar$ geochronological analyses, after irradiation in TRIGA Reactor at the Oregon State University (USA) or US Geological Survey nuclear reactor (Denver, USA), groundmass and mineral separates were analysed by laser step-heating with (i) ARGUS VI (samples BAL1, BAL7, TER1, BOL1, LB1, and EU52) and (ii) MAP 215–50 (samples EU4, EU5B, EU8B, and EU13A) mass spectrometers at Curtin University within the Western Australian Argon Isotope Facility (WAAIF) of the John de Laeter Centre and (iii) Nu Instruments Noblesse magnetic sector noble gas mass spectrometer (samples BI14 and 25B) at the Noble Gas Lab of the University of Vermont. Extended analytical procedures and details are reported in section S1 of the Supplementary materials.

7. Petrography and rock classification

Samples BAL7, BI14 (Val d'Adige district), BOL1 (Lessini Mts. district), LB1, and 25B (Marosticano district) are nepheline-normative and they are classified as basanites in the total alkali vs. silica (TAS) diagram (Le Maitre et al., 2002; Table 1; Fig. 3). These rocks show porphyritic texture with large (up to 1 mm across) phenocrysts of euhedral olivine and smaller clinopyroxene (prevalently diopside; up to 0.5 mm across) as dominant phenocrysts set in a microcrystalline groundmass constituted by acicular plagioclase, clinopyroxene, and oxides. Interestingly, BOL1, LB1, and 25B host small (3–4 mm) spinel peridotite xenoliths, probably fragments of the bigger (5–15 cm) counterparts already discovered in alkaline basalts of the Val d'Adige, Lessini Mts., and Marosticano districts (Morten et al., 1989; Siena and Coltorti, 1989, 1993; Beccaluva et al., 2001; Gasperini et al., 2006; Brombin et al., 2018). These xenolithic fragments were extracted from the samples before proceeding with the chemical analysis.

BAL1 (Val d'Adige district) and TER1 (Lessini Mts. district) are two basalts according to the TAS classification (Fig. 3). The first sample is olivine/hyperstene normative, while the second one is quartz-normative (Table 1). Both rocks have intergranular texture characterized by elongated and euhedral plagioclase (up to 2 mm across) and subhedral-anhedral clinopyroxene, olivine and oxides filling spaces between

Table 1
Whole-rock major element compositions (wt%) and CIPW normative compositions of the VVP magmatic products.

Sample	BAL1	BAL7	BI14	TER1	BOL1	EU1AB	EU53	EU52	EU8B
Rock	Basalt	Basanite	Basanite	Basalt	Basanite	Basaltic andesite	Basaltic andesite	Basaltic trachyandesite	Basaltic trachyandesite
District	Val d'Adige	Val d'Adige	Val d'Adige	Lessini Mts.	Lessini Mts.	Euganean Hills	Euganean Hills	Euganean Hills	Euganean Hills
Sampling coordinates	45°47′02″N 10°54′18″E	45°44′37″N 10°53′04″E	45°47′02″N 10°54′18″E	45°35′34″N 11°12′58″E	45°35′51″N 11°12′31″E	45°19′40″N 11°38′58″E	45°32′87″N 11°68′48″E	45°32′87″N 11°68′48″E	45°19′07″N 11°46′31″E
SiO_2	46.83	42.62	42.01	48.72	43.00	52.00	53.22	51.70	55.63
TiO_2	2.75	3.71	3.22	2.80	3.44	2.45	2.37	2.75	2.01
Al_2O_3	14.59	13.04	14.65	13.53	13.21	14.85	14.83	16.29	15.53
Fe_2O_{3tot}	14.61	14.56	13.11	11.00	14.35	10.02	11.24	10.43	8.82
MnO	0.20	0.19	0.17	0.36	0.19	0.12	0.12	0.12	0.13
MgO	6.94	8.96	8.28	10.77	9.55	6.25	6.22	3.85	3.41
CaO	10.39	11.03	10.34	9.93	10.23	9.50	8.66	6.12	6.47
Na_2O	2.24	3.09	4.98	1.09	3.06	3.10	3.24	4.35	4.23
K_2O	0.75	1.37	1.42	1.17	1.45	0.59	0.43	3.23	2.68
P_2O_5	0.70	1.53	1.81	0.64	0.97	0.35	0.26	0.97	0.59
Tot	100.01	100.10	100.00	100.00	99.45	99.23	100.59	99.81	99.50
LOI	3.02	1.10	2.17	3.30	0.55	3.69	3.11	0.83	2.34
mg#	49.32	55.77	56.40	66.72	57.69	56.10	53.13	43.06	44.20
Quartz	–	–	–	1.4	–	2.6	4.4	–	2.6
Nepheline	–	7.9	18.3	–	8.2	–	–	0.43	–
Diopside	16.2	22.3	21.6	13.4	21.8	16.5	13.6	7.2	10.6
Hyperstene	16.1	–	–	30.9	–	18.1	19.6	–	11.6
Olivine	6.0	18.0	15.3	–	19.5	–	–	11.2	–

Sample	EU13A	EU4	EU5B	EU9	LB1	25B
Rock	Latite	Trachyte	Rhyolite	Rhyolite	Basanite	Basanite
District	Euganean Hills	Euganean Hills	Euganean Hills	Euganean Hills	Marosticano	Marosticano
Sampling coordinates	45°15′07″N 11°41′27″E	45°20′20″N 11°39′06″E	45°19′16″N 11°45′24″E	45°14′57″N 11°44′28″E	45°76′72″N 11°67′78″E	45°76′72″N 11°67′78″E
SiO_2	56.90	65.52	69.86	72.00	43.22	44.02
TiO_2	2.00	0.69	0.39	0.32	3.47	3.12
Al_2O_3	15.68	16.51	15.41	14.81	11.52	12.80
Fe_2O_{3tot}	7.27	3.71	2.05	1.26	13.12	10.95
MnO	0.09	0.06	0.09	0.03	0.19	0.16
MgO	3.14	0.72	0.17	0.14	11.29	12.26
CaO	5.68	1.59	0.65	0.49	11.85	10.89
Na_2O	4.11	5.23	4.80	4.63	3.06	3.22
K_2O	3.59	5.11	5.77	5.56	1.36	1.53
P_2O_5	0.57	0.30	0.07	0.03	0.97	1.06
Tot	99.03	99.44	99.26	99.27	100.05	100.00
LOI	1.64	0.35	0.66	0.14	1.17	1.08
mg#	46.95	28.45	14.52	18.54	63.81	69.64
Quartz	3.5	10.3	17.6	22.3	–	–
Nepheline	–	–	–	–	11.0	10.4
Diopside	9.0	–	–	–	31.5	25.1
Hyperstene	9.8	5.6	2.6	1.5	–	–
Olivine	–	–	–	–	17.9	20.1

mg# = $100 \times Mg/(Mg + Fe^{2+})_{mol}$ considering $Fe^{3+}/Fe^{2+} = 0.15$.

plagioclase crystals. The presence of scarce iddingsite (substituting for olivine) and amygdules of secondary hydrothermal minerals are indicative of slight alteration. According to the TAS diagram, EU1AB and EU53 (Euganean Hills district) are classified as basaltic andesites (Fig. 3). Both samples are quartz-normative (Table 1) and they have clinopyroxene, plagioclase, and oxides as phenocrysts and in the groundmass.

EU52 and EU8B (Euganean Hills district) are classified as basaltic trachyandesites in the TAS diagram (Fig. 3). EU52 is nepheline-normative, while EU8B is quartz-normative (Table 1). The phenocrysts of these two samples are plagioclase, amphibole, and clinopyroxene in a microcrystalline groundmass of plagioclase and oxides. The plagioclase phenocrysts (up to 2 mm across in EU8B and up to 5 mm across in EU52) are generally euhedral with occasional sieved-textured centers (EU8B). The clinopyroxene phenocrysts (up to 1 mm across) are subhedral with rounded edges. Only EU52 exhibits large (up to 5 mm across) euhedral amphibole without any sign of alteration.

The quartz-normative sample EU13A (Euganean Hills district) is classified as latite (Table 1; Fig. 3). It contains medium-grained (0.5–1.5 mm across) plagioclase, biotite, and clinopyroxene in a microcrystalline groundmass of plagioclase feldspar and oxides. The plagioclase phenocrysts (up to 1.5 mm across) are generally euhedral and display a sieved-textured core. The clinopyroxene crystals (1 mm across) are subhedral with rounded edges. Biotite (1 mm across) is subhedral and partly replaced by oxides along the rims.

EU4, EU5B, and EU9 (Euganean Hills district) are the most felsic samples of the entire suite. According to the TAS diagram, EU4 is a trachyte, whereas EU5B and EU9 are rhyolites (Fig. 3). All of them are quartz-normative (Table 1). They exhibit glomeroporphyritic texture and the phenocrysts are predominantly alkali feldspar (sanidine; up to 5 mm across), plagioclase (up to 5 mm across), and biotite (1–2 mm across) in a microcrystalline groundmass consisting of alkali feldspar and Fe–Ti oxides. Phenocrysts of amphibole (1–2 mm across) are present only in the EU4. The glomerocrysts, up to 1 cm in diameter, are both monomineralic (alkali feldspar) or formed by plagioclase and alkali feldspar in the same cluster. Crystals within these glomerocrysts are subhedral with rounded corners on the edges of grains.

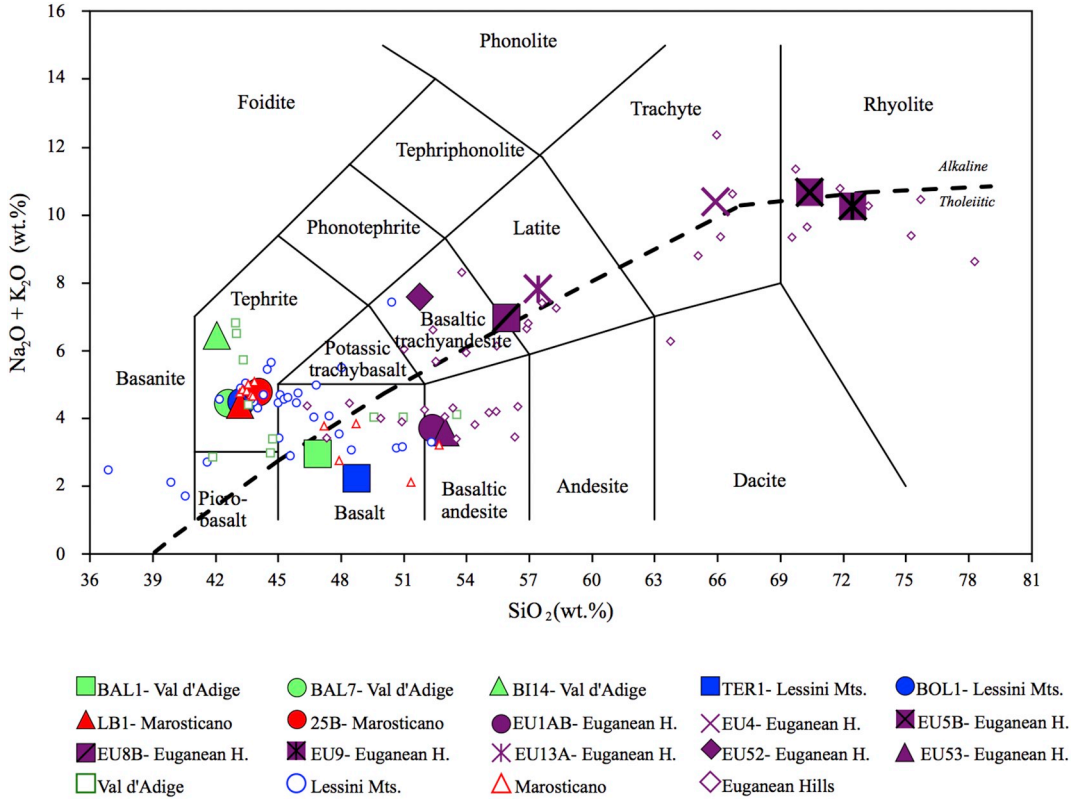

Fig. 3. Total Alkali vs. Silica (TAS) classification diagram (Le Maitre et al., 2002) of the magmatic products from Val d'Adige, Lessini Mts., Marosticano, and Euganean Hills studied in this work (large symbols) and from previous studies (small symbols). The Val d'Adige samples are from Beccaluva et al. (2007); the Lessini Mts., and the Marosticano samples are from Macera et al. (2003) and Beccaluva et al. (2007); the Euganean Hills samples are from Milani et al. (1999) and Macera et al. (2003). The trachybasalt and trachyandesite fields are labelled here "potassic trachybasalt" and "latite", respectively, as most of the VVP samples has potassic affinity [$(Na_2O - K_2O) \leq 2.0$] following the Le Maitre et al. (2002) nomencalture. The alkaline-tholeiitic discrimination line is from Irvine and Baragar (1971).

Table 2
Trace element (ppm) compositions of the VVP magmatic products.

Sample	BAL7	TER1	BOL1	EU1AB	EU53	EU52	LB1
Rock	Basanite	Basalt	Basanite	Basaltic andesite	Basaltic andesite	Basaltic trachyandesite	Basanite
District	Val d'Adige	Lessini Mts.	Lessini Mts.	Euganean Hills	Euganean Hills	Euganean Hills	Marosticano
Rb	29.6	27.8	37.4	17.0	15.0	71.0	46.6
Ba	860	664	553	348	264	777	777
Th	6.80	5.87	5.99	2.95	2.85	10.1	6.85
U	1.77	1.34	1.42	0.83	0.82	2.56	2.00
Nb	124	74.3	91.4	28.0	21.0	96.6	118
Ta	4.47	2.52	3.74	1.38	1.43	4.64	4.67
La	66.6	39.0	47.0	18.4	13.7	72.4	57.5
Ce	131	75.8	96.1	38.5	28.5	128	109
Pr	15.5	8.37	11.5	4.68	3.71	14.4	12.1
Sr	1744	736	1060	473	349	929	1071
Nd	67.4	35.6	52.0	20.4	16.9	55.9	53.3
Zr	413	235	354	175	168	456	382
Hf	8.29	5.01	7.58	3.93	4.03	9.11	7.91
Sm	12.6	6.73	10.1	5.36	4.85	10.9	9.68
Eu	3.86	2.16	3.13	1.83	1.75	3.25	2.91
Gd	11.7	6.66	9.32	5.55	5.47	8.82	8.92
Tb	1.64	0.99	1.38	0.83	0.85	1.19	1.27
Dy	7.20	4.63	6.23	4.48	4.77	6.15	5.61
Y	40.8	28.7	35.4	24.1	24.0	34.6	31.5
Ho	1.28	0.88	1.10	0.83	0.88	1.10	1.00
Er	3.05	2.22	2.62	1.97	2.20	2.64	2.42
Yb	2.21	1.84	1.93	1.56	1.70	2.03	1.78
Lu	0.31	0.27	0.27	0.21	0.23	0.27	0.25

All trace elements (ppm) were analysed by ICP-MS except Ba (XRF).

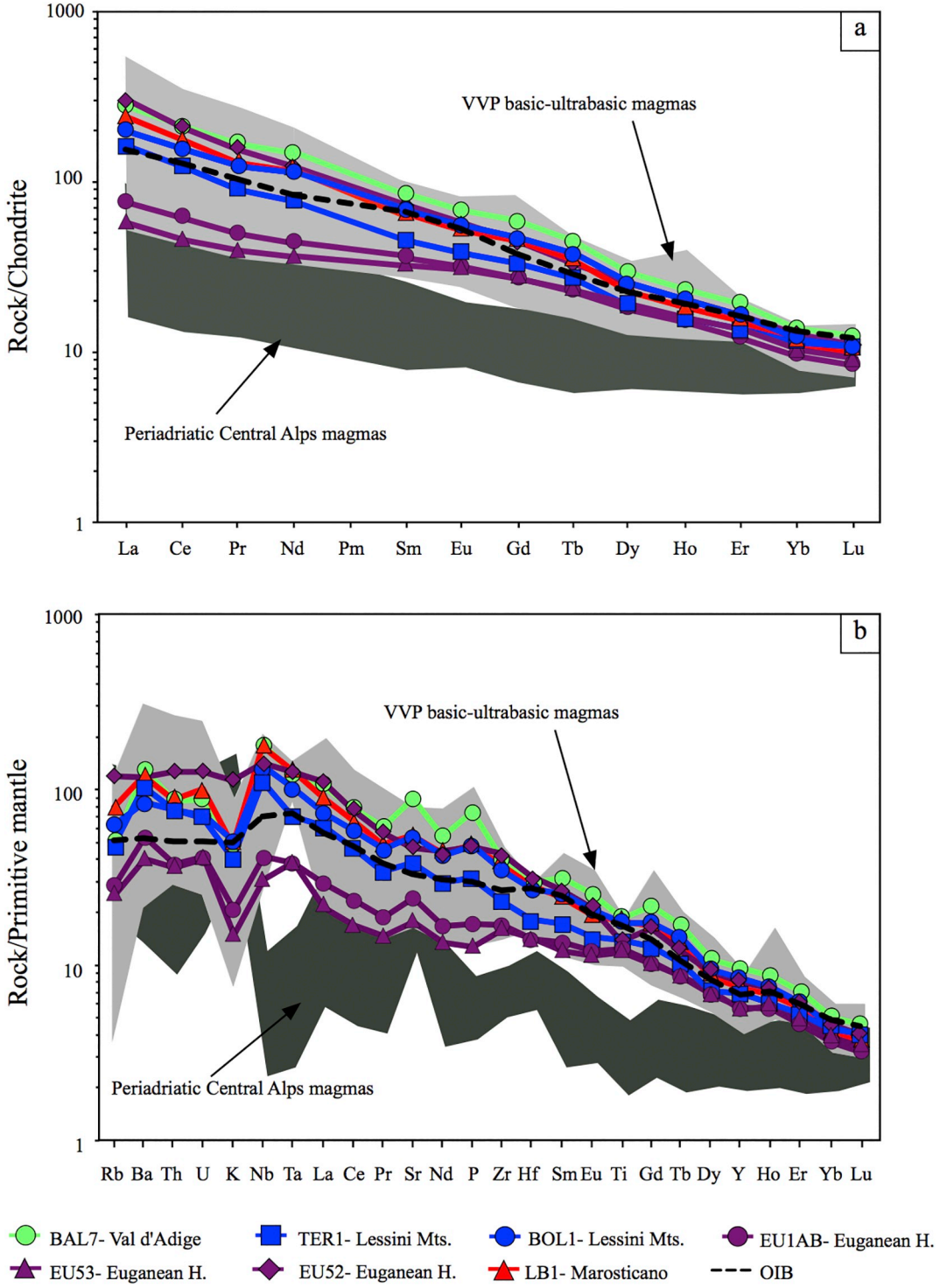

Fig. 4. Chondrite-normalized rare earth elements (a) and primitive mantle-normalized incompatible trace element patterns (b) of basic–ultrabasic rocks from Val d'Adige, Lessini Mts., Euganean Hills, and Marosticano. Previously published trace element compositions of VVP basic–ultrabasic rocks (light grey field; Macera et al., 2003; Beccaluva et al., 2007) and the trace element compositions of orogenic calc-alkaline and sub-alkaline magmas of the Periadriatic Central Alps magmatism (dark grey field; Bergomi et al., 2015) are also reported for comparison.

8. Geochemistry

Bulk major and trace element compositions of the analysed magmatic rocks are reported in Tables 1 and 2. On the TAS diagram (Fig. 3) this group of magmatic rocks overlaps with those previously published for the VVP (Milani et al., 1999; Macera et al., 2003; Beccaluva et al., 2007), spanning a wide range of compositions from alkaline to subalkaline and encompassing ultrabasic, basic, intermediate, and acid rocks.

The basic–ultrabasic rocks span a relatively wide range in terms of SiO_2 (42.01 to 55.63 wt%; Table 1), MgO (12.26 to 3.41 wt%; Table 1), and mg# [69.64 to 43.06, where mg# is defined as $100 \times Mg/(Mg + Fe^{2+})_{mol}$, Fe^{3+}/Fe^{2+} being 0.15; Table 1] reflecting the different degree of evolution of the VVP magmas (i.e., from basanites to

basaltic trachyandesites). The analysed samples have predominantly alkaline composition with the majority of the samples having potassic affinity [($Na_2O - K_2O$) ≤ 2.0 wt%] with ($Na_2O - K_2O$) ranging from −0.08 to 1.72 wt%. Only BI14, EU53, and EU1AB have sodic affinity [($Na_2O - K_2O$) = 2.51 to 3.48 wt%]. Chondrite-normalized rare earth element (REE) patterns are generally parallel for all basic–ultrabasic rocks (Fig. 4a). These patterns are strongly light REE (LREE) enriched with a significant LREE to heavy REE (HREE) fractionation [$(La/Yb)_N$ = 5.5 to 24.3; $(Dy/Lu)_N$ = 1.8 to 2.4; Fig. 4a]. Irrespective to the lithology, samples from Val d'Adige, Lessini Mts., Euganean Hills (EU1AB and EU53), and Marosticano exhibit negative Rb, K, Zr–Hf, and Ti anomalies and spikes of Ba, Sr, and P in the primitive mantle-normalized incompatible trace element diagram (Fig. 4b). The basaltic trachyandesite EU52 (Euganean Hills) mimics the general trace element features of the basic–ultrabasic samples, however, it lacks significant Sr and P spikes and it is depleted in Ba (Fig. 4b).

The intermediate-acid rocks (SiO_2 = 56.90 to 72.00 wt%; Table 1) have lower MgO (3.14 to 0.14 wt%; Table 1) with respect to the previous group, consistent with their more evolved nature. All these samples have potassic affinity [($Na_2O - K_2O$) = −0.97 to 1.55 wt%]. No trace element analyses were performed for this group of samples, as in this work we preferred to focus on the geochemistry of basic–ultrabasic samples that can shed light on their mantle sources, while more evolved rocks may be significantly affected by fractional crystallization.

Black dashed line is for Ocean Island Basalt composition (OIB; Sun and McDonough, 1989). Normalizing factors are from McDonough and Sun (1995). (For interpretation of the references to color in this figure legend, the reader is referred to the web version of this article.)

9. $^{40}Ar/^{39}Ar$ geochronological results

Detailed $^{40}Ar/^{39}Ar$ results of the analysed magmatic rocks are reported in Tables 3 and 4. Groundmass samples of BAL1, BAL7, TER1, BOL1, and LB1 as well as amphibole and plagioclase separates of EU52 were analysed with a new generation noble gas multicollector mass spectrometer (ARGUS VI). Instead, mineral separates (i.e., biotite, feldspar, and sanidine) from EU8B, EU13A, EU4, EU5B, and EU9 were analysed with the MAP215–50 mass spectrometer. EU1AB and EU53, two basaltic andesites from the Euganean Hills district, could not be dated due to the lack of fresh K-rich minerals. Many analysed samples are characterized by $^{40}Ar/^{36}Ar$ ratios, which are above or below the atmospheric value (298.56 ± 0.31; Lee et al., 2006). Supra-atmospheric intercepts are indicative of excess ^{40}Ar whereas sub-atmospheric ratios are too low to be due to isotopic fractionation (Oostingh et al., 2017) and are rather interpreted in term of hydrothermal alteration signature (Baksi, 2006). In addition, many samples yielded only mini-plateaus (50–70% cumulative ^{39}Ar; Jourdan et al., 2007). The latter are less robust than their plateau counterparts and should be treated with caution. They might indicate the true crystallization age, but they might equally represent minimum age values, not too far from the crystallization age (Oostingh et al., 2017). The complete description of the dating result is reported in section S2 of the Supplementary materials.

For the Val d'Adige, the basalt BAL1 and basanite BAL7 $^{40}Ar/^{36}Ar$ intercepts are similar and slightly sub-atmospheric (BAL1 = 266 ± 23 and BAL7 = 264 ± 15; Table 3; Fig. 5a, c), which allow equally calculating a plateau age of 41.69 ± 0.37 Ma (Table 3; Fig. 5b) and a mini-plateau age of 41.98 ± 0.20 Ma (Table 3; Fig. 5d), respectively.

TER1 and BOL1 were analysed for the Lessini Mts. district and yielded different $^{40}Ar/^{36}Ar$ and intercept ages. The basalt TER1 shows sub-atmospheric $^{40}Ar/^{36}Ar$ intercept (253 ± 25; Table 3; Fig. 5e) defining a mini-plateau age of 45.21 ± 0.11 Ma (Fig. 5f). The $^{40}Ar/^{36}Ar$ intercept of basanite BOL1 is 278 ± 19 (Table 3; Fig. 5g), close to the atmospheric $^{40}Ar/^{36}Ar$ ratio. This sample yielded a mini-plateau age of 38.73 ± 0.44 Ma (Table 3; Fig. 5h).

For the basaltic trachyandesite EU52 both amphibole and plagioclase were analysed. The amphibole is characterized by a $^{40}Ar/^{36}Ar$ intercept (295 ± 14; Table 3; Fig. 5i) indistinguishable from atmosphere, and yielded a mini-plateau age of 32.35 ± 0.09 Ma (Fig. 5j). The plagioclase $^{40}Ar/^{36}Ar$ intercept value is supra-atmospheric (397 ± 19; Table 3; Fig. 5k), indicating excess ^{40}Ar. Using the latter value, we obtained a plateau age of 32.16 ± 0.06 Ma (Table 3; Fig. 5l). The alkali-feldspar separate of the basaltic trachyandesite EU8B shows a value of 305 ± 99 (Table 3; Fig. 5m) for the $^{40}Ar/^{36}Ar$ intercept, which is indistinguishable from the atmospheric ratio and allows calculating a plateau age of 32.17 ± 0.32 Ma (Table 3; Fig. 5n). The

Table 3
Summary of $^{40}Ar/^{39}Ar$ results for VVP samples at Western Australian Argon Isotope Facility (WAAIF).

General characteristics				Isochron characteristics					Plateau characteristics			
Sample	Lithology	Instrument	Separate	Inverse isochron age (Ma, ± 2σ)	n	$^{40}Ar/^{36}Ar$ intercept (± 2σ)	MSWD	P (%)	Plateau age (Ma, ± 2σ)	Total ^{39}Ar released (%)	MSWD	P (%)
Val d'Adige												
BAL1	Basalt	ARGUS VI	Groundmass	**41.70 ± 0.82**	16	266 ± 23	0.78	69	**41.69 ± 0.37**	75	0.39	98
BAL7	Basanite	ARGUS VI	Groundmass	*41.95 ± 0.46*	15	264 ± 15	0.82	64	*41.98 ± 0.20*	60	0.25	100
Lessini Mts.												
TER1	Basalt	ARGUS VI	Groundmass	*45.21 ± 0.15*	12	253 ± 25	1.00	44	*45.21 ± 0.11*	57	0.83	61
BOL1	Basanite	ARGUS VI	Groundmass	*40.60 ± 1.76*	17	278 ± 19	0.75	74	*38.73 ± 0.44*	62	0.99	46
Euganean Hills												
EU52	Basaltic trachyandesite	ARGUS VI	Amphibole	*32.37 ± 0.12*	10	295 ± 14	0.52	85	*32.35 ± 0.09*	67	0.48	89
			Plagioclase	**32.16 ± 0.08**	21	397 ± 19	0.65	87	**32.16 ± 0.06**	100	0.58	93
EU8B	Basaltic trachyandesite	MAP 215–50	Feldspar	**32.11 ± 0.98**	15	305 ± 99	0.85	61	**32.17 ± 0.32**	100	0.79	68
EU13A	Latite	MAP 215–50	Feldspar	**31.96 ± 1.13**	14	349 ± 136	0.52	91	**32.34 ± 0.51**	88	0.53	91
EU4	Trachyte	MAP 215–50	Biotite	**31.83 ± 0.50**	14	328 ± 43	0.88	57	**32.09 ± 0.29**	100	0.97	48
EU5B	Rhyolite	MAP 215–50	Sanidine	**31.87 ± 0.79**	15	343 ± 58	0.86	59	**32.30 ± 0.52**	100	1.00	45
EU9	Rhyolite	MAP 215–50	Sanidine	**32.02 ± 0.67**	14	315 ± 68	0.51	91	**32.17 ± 0.27**	100	0.48	94
Marosticano												
LB1	Basanite	ARGUS VI	Groundmass	No isochron age					No plateau age			

Data in italics are derived from mini–plateaus (50–70% ^{39}Ar released) and are considered minimum ages only, bold font represents statistically significant plateau ages (> 70% ^{39}Ar released). Mean square weighted deviation (MSWD) for isochron, plateau, and mini–plateau, number of analyses included in the isochron, $^{40}Ar/^{36}Ar$ intercept, percentage of ^{39}Ar degassed used in the plateau calculation, probability (P) for isochron, plateau and mini–plateau are indicate. Analytical uncertainties on the ages and $^{40}Ar/^{36}Ar$ intercepts are quoted at 2 sigma (2σ) confidence levels.

Table 4
Summary of 40Ar/39Ar results of VVP two districts only, analysed at the Noble Gas Geochronology Laboratory of the University of Vermont with Nu Instruments Noblesse magnetic sector noble gas mass spectrometer.

General characteristics			Isochron characteristics				Plateau characteristics			
Sample	Lithology	Separate	Inverse isochron age (Ma, ± 2σ)	n	$^{40}Ar/^{36}Ar$ intercept (± 2σ)	MSWD	Plateau age (Ma, ± 2σ)	Total ^{39}Ar released (%)	MSWD	P (%)
Val d'Adige										
BI14	Basanite	Groudmass	*42.2 ± 8.2*	7	207 ± 138	11.3	*40.73 ± 0.48*	57	0.8	45
Marosticano										
25B	Basanite	Groudmass	No isochron age				No plateau age			

Data in italics are derived from mini-plateau (50–70% ^{39}Ar released) and are considered minimum ages only. Mean square weighted deviation (MSWD) for isochron and mini-plateau, number of analyses included in the isochron, $^{40}Ar/^{36}Ar$ intercept, percentage of ^{39}Ar degassed used in the plateau calculation and probability (P) for mini-plateau are indicated. Analytical uncertainties on the ages and $^{40}Ar/^{36}Ar$ intercept are quoted at 2 sigma (2σ) confidence levels.

feldspar separate of the latite EU13A yielded a $^{40}Ar/^{36}Ar$ intercept of 349 ± 136 (Fig. 5o) and a plateau age of 32.34 ± 0.51 Ma (Fig. 5p). The $^{40}Ar/^{36}Ar$ intercept age for the biotite separate of trachyte EU4 is 328 ± 43 (Table 3; Fig. 5q) and defines a plateau age of 32.09 ± 0.29 Ma (Fig. 5r). Also for the sanidine separate of rhyolite EU5B the $^{40}Ar/^{36}Ar$ intercept is slightly supra-atmospheric (343 ± 58; Fig. 5s); the calculated plateau age is 32.30 ± 0.52 Ma (Table 3; Fig. 5t). The sanidine separate of rhyolite EU9 shows a $^{40}Ar/^{36}Ar$ intercept value (315 ± 68; Table 3; Fig. 5u) indistinguishable from atmosphere and we obtained a plateau age of 32.17 ± 0.27 Ma (Table 3; Fig. 5v). It is clear that irrespective to the lithology all analysed Euganean samples yielded nearly indistinguishable ages, allowing calculate a mean weighted age of 32.21 ± 0.09 Ma.

The basanite from the Marosticano district, LB1, yielded the youngest integrated age of the VVP samples analysed at WAAIF using the ARGUS VI mass spectrometer. It did not return isochron and plateau age, but almost all the steps indicate apparent ages between 23.2 and 20.5 Ma (Table 3; Fig. 5w, x).

Two additional basanites BI14 and 25B, from the Val d'Adige and the Marosticano districts, respectively, were analysed at the Noble Gas Geochronology Laboratory of the University of Vermont using the Nu Instruments Noblesse magnetic sector noble gas mass spectrometer with the purpose to expand the VVP geochronological dataset. Sample BI14 yielded a $^{40}Ar/^{36}Ar$ intercept of 207 ± 138 and a mini-plateau age of 40.73 ± 0.48 Ma (Table 4; Fig. 6a, b). This age is similar to those recorded by BAL1 and BAL7. As occurred for LB1, also the Marosticano basanite 25B did not provide ages (Table 4; Fig. 6c, d). However, for both Marosticano samples almost all the steps indicate apparent ages of ~23–22 Ma (Fig. 6d).

10. Discussion

10.1. The mantle source of VVP magmatism

Most analysed magmatic products of the VVP show mg# significantly lower than typical primary magmas (Table 1), i.e., they have undergone at least some fractional crystallization before being erupted to the surface. However, at least a few rocks have mg# higher than 55 and, as mentioned before, host millimeter to centimeter-sized fragments of peridotite xenoliths, which point to fast transport of magma from mantle depths to the surface. Conservatively, we consider only the trace elements contents of the less evolved VVP samples exhibiting MgO > 8 wt% and mg# > 55 (BAL7, TER1, BOL1, and LB1) to constrain the nature and evolution of their mantle source. The selected samples are characterized by low LILE/HFSE, LREE/HFSE ratios, and high-Nb contents (Fig. 4b). Notably, also slightly more evolved basic samples, including most of those from the Euganean Hills, display similar trace element features, indicating that the described geochemical features are common within the entire VVP, i.e. similar mantle source signatures for the entire province. The trace element and REE patterns of the VVP samples are clearly distinct from those of the Periadriatic Central Alps calc-alkaline and sub-alkaline products with arc signature (Bergomi et al., 2015; Fig. 4a, b) and are instead consistent with the within-plate features already noticed in previous studies on the VVP (Milani et al., 1999; Beccaluva et al., 2007; Macera et al., 2008; Fig. 4a, b). In fact, Beccaluva et al. (2001, 2007) invoked an Ocean Island Basalts (OIB)-like mantle source (Sun and McDonough, 1989) for these magmas, justifying the deviations of VVP samples from typical OIB trace element patterns (Fig. 4a, b) with the identification of a spinel lherzolite enriched with hydrated-carbonated components as potential source.

The basaltic trachyandesite from the Euganean Hills (EU52; Fig. 4a, b) represents an exception. This sample is the only one of the VVP suite that displays an OIB-like REE pattern, with no significant negative K and Rb anomalies, reflecting a possible compositional variation of the mantle source (or crustal contamination?) within the Euganean district. However, due to its more evolved character (mg# = 43 and MgO = 3.85 wt%; Table 1), we preferred to exclude this sample from our geochemical models.

Using the geochemical features of the sample suite of this study we estimated: (i) the depth of the partial melting region; (ii) the mineralogical and geochemical features of the melting mantle source(s); and (iii) the geodynamic evolution that may be responsible for the enrichment/depletion processes in the VVP mantle source region.

10.1.1. Mantle modelling

To evaluate whether the trace element features of the alkaline rocks (i.e., LREE enrichments, negative K–Rb, Zr, Hf, and Ti anomalies) from the VVP are inherited from their mantle source(s) we performed various partial melting trace-element modelling. The trace element patterns and ratios of the selected VVP basic–ultrabasic rocks were at first used to constrain the depth of the VVP mantle source, i.e., if it was in the garnet or in the spinel stability field as suggested for example by Beccaluva et al. (2007). The steep middle (M)–HREE profiles of the selected VVP samples suggest a possible presence of garnet in the mantle source, as this mineral progressively takes up the HREE over MREE ($^{garnet/melt}Kd_{Sm}/^{garnet/melt}Kd_{Yb} \sim 10^{-3}$; e.g., van Westrenen et al., 2001; Niu et al., 2011). When garnet is no longer stable, clinopyroxene becomes the sole anhydrous peridotitic phase that can accommodate REE (Hellebrand et al., 2002). This mineral has an almost equal partition coefficient for MREE and HREE during melting ($^{clinopyroxene/melt}Kd_{Sm}/^{clinopyroxene/melt}Kd_{Yb}$ close 1.0; Green et al., 2000; Niu et al., 2011), imposing melt REE profiles with almost flat M–HREE patterns. Taking this into account, values of $(Sm/Yb)_N$ higher than 1.0 are considered evidence for garnet signature in OIBs (Niu et al., 2011). Such consideration may apply also to VVP basic–ultrabasic samples [$(Sm/Yb)_N$ = 3.9 to 6.1].

Lanthanum is highly incompatible during melting and difficult to accommodate in both garnet and clinopyroxene. This implies that any fertile or moderately fertile mantle source in the early stages of melting produces melts with positive fractionated REE pattern [$(La/Yb)_N$ > > 1] in both garnet or spinel stability fields. However, by combining REE ratios such as La/Yb and Dy/Yb, it is possible to

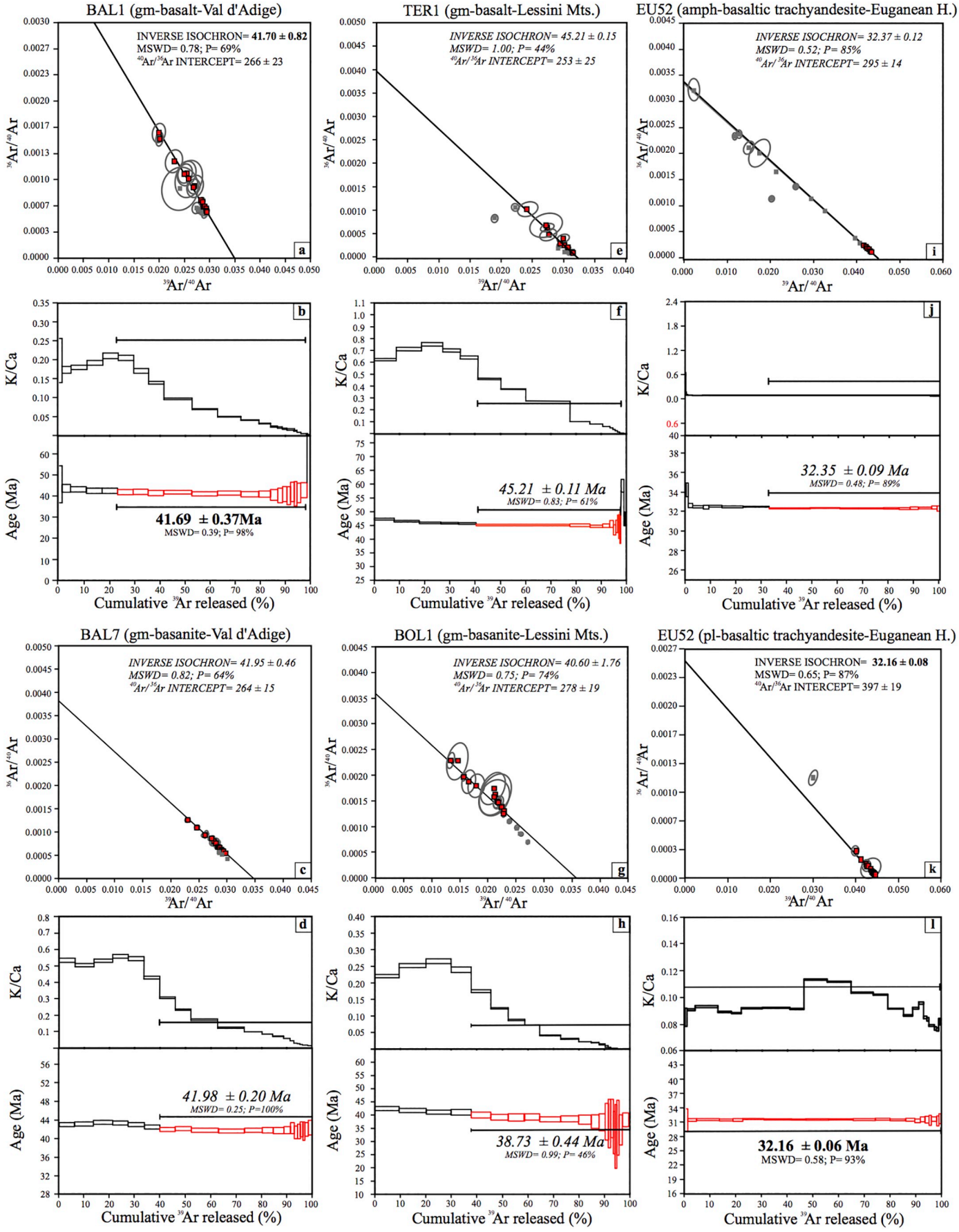

(caption on next page)

Fig. 5. $^{39}Ar/^{40}Ar$ vs. $^{36}Ar/^{40}Ar$ inverse isochrons and $^{40}Ar/^{39}Ar$ apparent age and K/Ca spectra, plotted against the cumulative percentage of ^{39}Ar released for VVP rocks. Plateau ages (bold) are inverse isochron intercept corrected. Mini-plateaus (50–70% cumulative ^{39}Ar) are indicated in italics. Mean square weighted deviation (MSWD) and probability of fit (P) are indicated. Errors on plateau ages are quoted at 2σ and do not include systematic errors (i.e., uncertainties on the age of the monitor and on the decay constant). These plots are obtained at Curtin University within the Western Australian Argon Isotope Facility (WAAIF) of the John de Laeter Centre using ARGUS VI and MAP 215–50 mass spectrometers.
Abbreviations: gm = groundmass; bt = biotite; san = sanidine; fsp = feldspar; pl = plagioclase; amph = amphibole.

constrain the presence or absence of garnet in the mantle source and consequently inferring the melting depth (e.g., Thirlwall et al., 1994). In fact, Dy/Yb is fractionated in the presence of residual garnet and this effect is seen for relatively high degrees of melting (Bogaard and Wörner, 2003). On the contrary, the presence of spinel in the source does not significantly fractionate La, Dy, and Yb ($^{spinel/melt}Kd_{La,\ Dy,\ Yb} \sim 10^{-4}$) as these elements are all moderately incompatible in this mineral. Therefore, in the spinel stability field, La/Yb is only slightly fractionated for small degrees of melting, and Dy/Yb is not fractionated at all (Bogaard and Wörner, 2003).

Notwithstanding the uncertainties related to the chosen parameters (trace element Kds, source composition, source mineralogy, etc.), the proposed melting models for the VVP (Fig. 7) clearly indicate that for the selected samples (and for the VVP in general) partial melting occurred within the garnet-peridotite stability field, i.e., at depths greater than about 70 km (e.g., Green and Ringwood, 1970; Frost, 2008; Ziberna et al., 2013). However, the melting of primitive mantle-like garnet-bearing fertile lherzolite is not suffice to provide the geochemical features of the majority of VVP basic–ultrabasic samples, which instead require a mantle source enriched in REE with respect to a fertile garnet lherzolite (Fig. 7).

Although all the selected basic–ultrabasic samples have a slight potassic affinity, in most of the primitive mantle-normalized multi-element patterns K and Rb are depleted, whereas Ba is enriched with respect to neighboring elements, and Zr, Hf, and Ti are always depleted with respect to the OIBs average (Fig. 4b). Such features suggest the presence of a residual K (Rb)-bearing phase (i.e., amphibole and/or phlogopite) in the mantle source (Greenough et al., 1988; Wilson and Downes, 1992; Moine et al., 2001), that was diluted in HFSE. This points to involvement of CO_2 rich melts or carbonatites as metasomatising agents in the VVP mantle source (Zanetti et al., 1999; Scott et al., 2016). In fact, all samples plot among the melting curves calculated for amphibole or phlogopite carbonated garnet lherzolite and that of the anhydrous garnet lherzolite. In general, the basanitic samples and most of the least evolved alkaline lavas from the Lessini Mts. (data from Beccaluva et al., 2007) would correspond to low degree melts (~1.5–4% melting) of a carbonated phlogopite-bearing mantle source, while the sub-alkaline (tholeiitic) samples suggest in general slightly higher melting degrees of mantle source(s) bearing-garnet. Only one Lessini Mts. tholeiite (Beccaluva et al., 2007) may be compatible with ~3–4% melting of a garnet-lherzolite (Fig. 7).

Since geophysical data indicate the depth of lithosphere-asthenosphere boundary under the VVP at ~100 km (Panza and Suhadolc, 1990), melting probably occurred within the deep lithosphere, in the garnet-stability field. This is also consistent with the inferred presence in the VVP mantle source of phlogopite or amphibole, minerals stabilized in a $CO_2 + H_2O$ system that would rapidly melt out in the asthenospheric mantle wedge (Frost, 2006, and references therein).

Unlike VVP basanites and basalts, the calc-alkaline and sub-alkaline basic dykes and intrusive rocks from the Periadriatic Central Alps magmatism exhibit flat HREE profiles (Bergomi et al., 2015; Fig. 4a, b) more consistent with a spinel-bearing peridotite, with scarce or absent contribution of metasomatic component (Fig. 7). This implies a relatively shallower melting depth for the orogenic compared to the intraplate VVP magmas.

The initial source and melting mineral modes of the source minerals are reported in Table 5.

Mineral melt distribution coefficients used for modelling are: $D_{olivine}^{La,\ Dy,\ Yb}$ 0.0002, 0.007, 0.0015; $D_{orthopyroxene}^{La,\ Dy,\ Yb}$ 0.0031, 0.022, 0.042; $D_{clinopyroxene}^{La,\ Dy,\ Yb}$ 0.049, 0.330, 0.300; $D_{garnet}^{La,\ Dy,\ Yb}$ 0.0014, 1.06, 4.01; $D_{spinel}^{La,\ Dy,\ Yb}$ 0.0001, 0.0001, 0.0001; $D_{phlogopite}^{La,\ Dy,\ Yb}$ 0.028, 0.097, 0.179; $D_{amphibole}^{La,\ Dy,\ Yb}$ 0.039, 0.406, 0.349. These values were selected from GERM website (http://earthref.org/).

10.1.2. Is phlogopite really the K (Rb)-bearing residual phase in the VVP mantle source?

The negative K and Rb anomalies shown by VVP samples (Fig. 4b) are possibly explained by residual phlogopite and amphibole in their mantle source, with the predominance of the former, taking also into account the REE distributions (Fig. 4a, b). Basanitic melts derived from sole amphibole-bearing mantle source are fingerprinted by a typical convex-upward pattern in the MREE (Meyzen et al., 2016), due the preference of MREE (Gd to Ho) relative the HREE (Er to Lu) of calcic amphiboles (Tiepolo et al., 2007). These features are not observed for VVP samples. On the contrary, evidence for the presence of phlogopite as the K-bearing residual phase is the Ba/Rb ratio. Both Rb and Ba are more compatible in phlogopite ($^{phlogopite/melt}D_{Rb} = 2.48$, $^{phlogopite/melt}D_{Ba} = 3.68$; LaTourette et al., 1995) than in amphibole ($^{amphibole/melt}D_{Rb} = 0.85$, $^{amphibole/melt}D_{Ba} = 1.0$; LaTourette et al., 1995). Considering these partition coefficients, melts formed from amphibole-bearing peridotites have higher Ba/Rb ratio (> 50), than melts of a phlogopite-bearing peridotites (Ba/Rb < 20; Furman and Graham, 1999; Zanazzi and Pavese, 2002; Tiepolo et al., 2007; Gatta et al., 2011; Meyzen et al., 2016). The relatively low Ba/Rb values (10 to 20) of most VVP basic–ultrabasic products thus support the presence of residual phlogopite rather than of amphibole within their mantle source.

10.1.3. The origin of the VVP mantle source enrichment

The basic–ultrabasic VVP magmatic products exhibit positive P anomalies associated with spikes of Ba and Sr (Fig. 4b). Such association has been described in within-plate magmatic suites generated from an enriched mantle source metasomatised by CO_2-rich fluids, which are able to carry Ba, Sr, and P (Yaxley et al., 1991; Ionov et al., 1996; Beccaluva et al., 2007; Dixon et al., 2008). For example, Merle et al. (2017) suggested that basic–ultrabasic alkaline magmatic rocks from Cameroon, which are geochemically characterized by enrichments in LREE, Ba, Sr, and P and depletions in Zr, were derived from a mantle source that underwent metasomatism from carbonatitic melts.

In the case of VVP basic–ultrabasic magmatic rocks, CO_2-rich fluids may have been provided by the subduction of the Tethys oceanic slab, which included calcareous metasediments and carbonated metabasics (Malusà et al., 2018). Following the latter authors, this subduction was "cold" allowing for major amounts of subducted carbonates to survive decarbonation and to be delaminated and stored at depths > 180 km, generating a long low velocity layer from the Central to the Eastern Southalpine domains (Malusà et al., 2018). In fact, according to Maierov et al. (2018) in any collision-subduction process, if the subducted sediments detach from the slab at great depth (> 100 km), their exhumation will be hindered by the thick overlying lithosphere and the subducted materials are forced to flow laterally forming a "long sheet" under the upper plate.

Malusà et al. (2018) proposed that after emplacement of the slab-derived carbonates under the base of the Adria microplate lithosphere, breakdown of these carbonates occurred due to the progressive rise of mantle temperatures at the slab interface. The new generated CO_2-rich melts, characterized by low density and viscosity (Frezzotti et al., 2009;

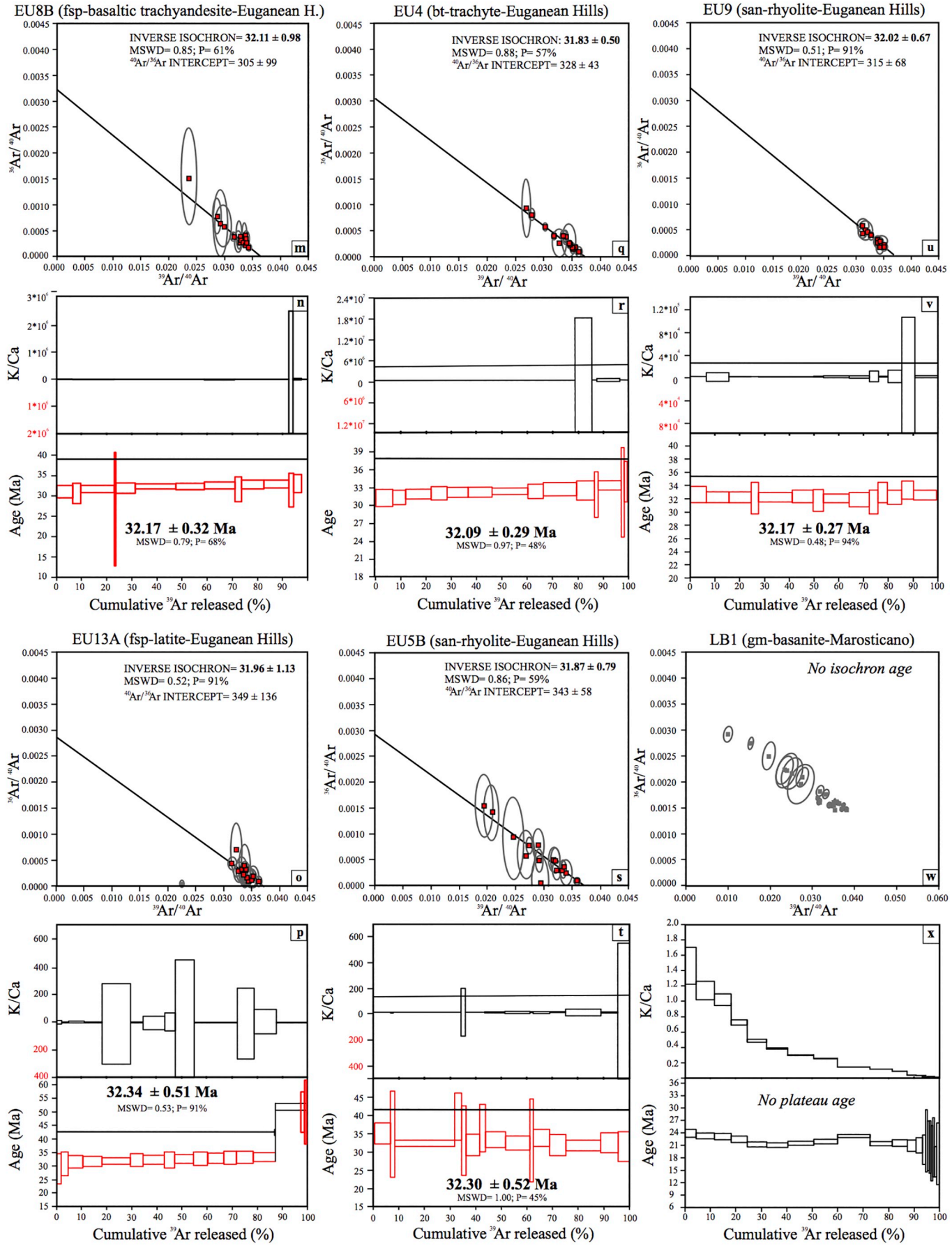

Fig. 5. (*continued*)

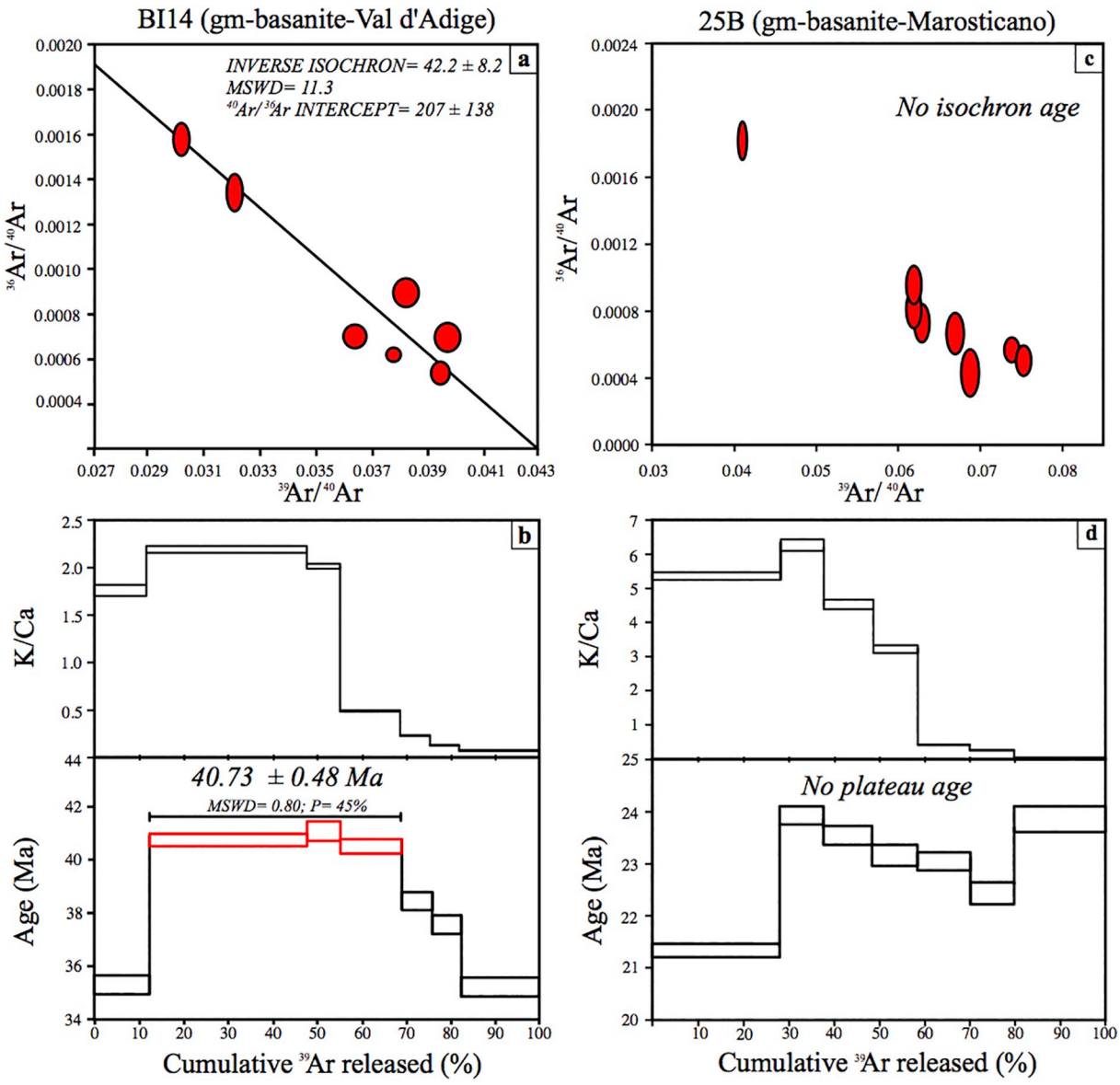

Fig. 6. $^{39}Ar/^{40}Ar$ vs. $^{36}Ar/^{40}Ar$ plot and $^{40}Ar/^{39}Ar$ apparent age and K/Ca spectra, plotted against the cumulative percentage of ^{39}Ar released for VVP rocks. The mini-plateau age is inverse isochron intercept ($^{40}Ar/^{39}Ar$) corrected and indicated in italics. Mean square weighted deviation (MSWD) and probability of fit (P) are reported. Error on the plateau age is quoted at 2σ. These plots are obtained at the Noble Gas Geochronology Laboratory of the University of Vermont with Nu Instruments Noblesse magnetic sector noble gas mass spectrometer.
Abbreviations: gm = groundmass.

Malusà et al., 2018), may have upwelled and infiltrated the overlying (garnet-bearing) mantle domain.

Furthermore, the metasomatic infiltration of CO_2-rich melts could be consistent with the presence of phlogopite in the mantle-source of the VVP, suggested by the LILE composition of these magmas (Moine et al., 2001). Several authors (e.g., Aulbach et al., 2004; Su et al., 2010; Meyzen et al., 2016; Sokol et al., 2017) invoked metasomatic processes of silicatic and/or carbonatitic melts and/or fluids to explain the presence of phlogopite in mantle sources. Similarly, we can think that the presence of phlogopite in the VVP mantle source could be responsible for the formation and stabilization of the potassic phase.

To summarize, the trace element data seem to indicate that VVP magmas were derived by partial melting of carbonated phlogopite-bearing garnet lherzolite (basanitic magmas). It is worth noticing that, except for a carbonatitic signature recorded in Marosticano mantle xenoliths (Brombin et al., 2018), the Val d'Adige and Lessini Mts. mantle xenoliths show no evidence of carbonatitic metasomatism. Therefore, we have not enough elements to constrain the age of the carbonatitic metasomatism recorded in the VVP magmatic products. However, according to Macera et al. (2003) and Beccaluva et al. (2007), the VVP melts are characterized also by low $^{87}Sr/^{86}Sr$ and high $^{143}Nd/^{144}Nd$ isotopic compositions, as typical of magmas derived from incompatible element depleted mantle sources. Such decoupling of enrichment in trace elements and depletion in isotopic compositions observed for the VVP magmatic products indicates that the carbonatitic metasomatic enrichment event must have occurred recently enough to be unable to significantly affect the isotope composition of the VVP magmas. This consideration emphasises our suggestion that the infiltration of carbonate fluids in the VVP mantle portion could have occurred after the breakdown of carbonates during the subduction of Tethys oceanic slab.

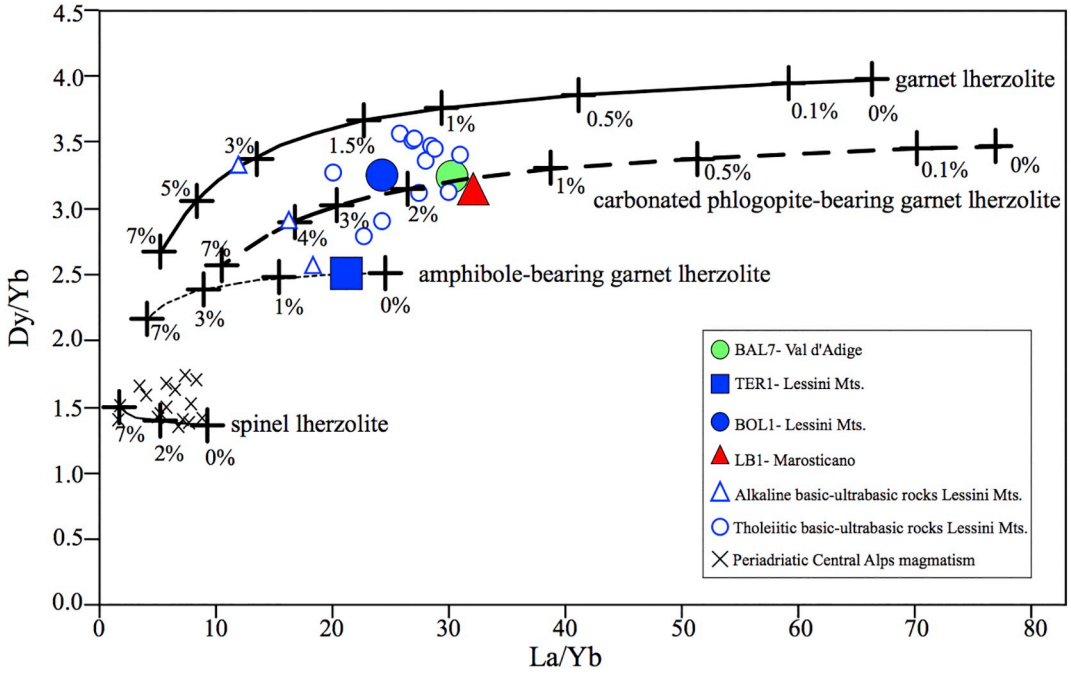

Fig. 7. Dy/Yb vs. La/Yb in selected basic–ultrabasic VVP samples from this study (large solid symbols) and from Beccaluva et al. (2007; small open symbols); orogenic calc-alkaline and sub-alkaline magmas of the Periadriatic Central Alps magmatism (small "x") are from Bergomi et al. (2015). All plotted samples have MgO > 8 wt% and mg# > 55. Non modal batch partial melting trajctories are shown for different mantle sources: garnet lherzolite (thick continuous line); carbonated phlogopite-bearing garnet lherzolite (thick dashed line); amphibole-bearing garnet lherzolite (thin dashed line); spinel lherzolite (thin continuos line). Tick marks on trajectories indicate melting degree.

10.2. The temporal evolution of the magmatic activity of the VVP

For basic–ultrabasic rocks older than Quaternary, the dating of mineral separates is preferred over groundmass for which separation of altered from fresh grains is difficult during sample preparation (Jourdan et al., 2007; Verati and Jourdan, 2013). However, due to the lack of relatively abundant and fresh phenocrysts of K-rich minerals in the VVP basanitic and basaltic samples, groundmass dating was carried out. For these samples, slight alteration is suggested by (i) the $^{40}Ar/^{36}Ar$ intercepts substantially lower than atmospheric values for VVP whole-rock data (< 298.56 ± 0.31; Table 3; Fig. 5a, c, e, g), (ii) the absence of proper plateau ages (i.e., < 70% ^{39}Ar released; Tables 3 and 4; Figs. 5d, f, h, j, x and 6b, c), and (iii) convex K/Ca spectra (Figs. 5b, d, f, h and 6b, d). In view of this, all the obtained mini-plateau ages are considered as minimum crystallization ages. However, the geological significance of these minimum ages is reinforced and confirmed by biostratigraphic data, when available. Therefore, we are confident that the reported whole-rock ages approximately constrain the actual crystallization ages, but we are aware that the true eruption age of a rock that yielded a mini-plateau could lie well outside of the 95% confidence level given by the sample uncertainties. Only Marosticano groundmass data did not define any isochron or plateau ages. However, the age spectra indicating a crystallization age of ~ 23–22 Ma (Figs. 5w, x and 6c, d) are confirmed by biostratigraphic data supporting a late Oligocene to early Miocene eruption in this district. Ages for the Euganean samples were all obtained on mineral separates and are thus of higher quality. All Euganean samples yielded statistically robust plateau ages based on > 88% of gas released (Table 3; Fig. 5l, n, p, r, t, v), only the amphibole separate from EU52 yielded a mini–plateau age (defined by 67% of the released gas; Table 3; Fig. 5j).

Based on the new age determinations and considering the available biostratigraphic data, we reconstructed the temporal evolution of the

Table 5
Source and melting mineral phases used in the non-modal batch model. Source compositions: Pyrolite REE composition of McDonough and Sun (1995) is chosen for all the partial melting scenario; carbonated phlogopite-bearing mantle source is estimated adding 0.025 mol fractions carbonatite in the initial source (La = 228 ppm; Dy = 3.28 ppm; Yb = 1.37 ppm) (Deng et al., 2017).

	Olivine	Orthopyroxene	Clinopyroxene	Garnet	Spinel	Phlogopite	Amphibole
Garnet lherzolite							
Mode of the source	0.57	0.20	0.15	0.08	—	—	—
Melting mode	0.05	0.20	0.30	0.45	—	—	—
Spinel lherzolite							
Mode of the source	0.57	0.22	0.18	—	0.03	—	—
Melting mode	0.10	0.20	0.55	—	0.15	—	—
Carbonated phlogopite-bearing garnet lherzolite							
Mode of the source	0.56	0.19	0.14	0.05	—	0.06	—
Melting mode	0.15	0.18	0.27	0.10	—	0.30	—
Amphibole-bearing garnet lherzolite							
Mode of the source	0.56	0.19	0.14	0.05	—	—	0.06
Melting mode	0.17	0.19	0.27	0.02	—	—	0.35

Cenozoic magmatism occurred in the Southeastern Alpine domain (Fig. 2). The VVP magmatic activity was discontinuous and took place with several pulses, covering a time-span of about 30 My (from late Paleocene to early Miocene). The oldest activity was always subaqueous, thus difficult to date by the $^{40}Ar/^{39}Ar$ technique due to the pervasive alteration of the volcanic products. However, biostratigraphic data constrain the Paleocene onset of VVP magmatism in the Val d'Adige and the Lessini Mts., as well as a late Eocene onset in the Euganean Hills (Piccoli et al., 1976, 1981; Savelli and Lipparini, 1979; Luciani, 1989; De Vecchi and Sedea, 1995; Bassi et al., 2008). The oldest age here obtained with the $^{40}Ar/^{39}Ar$ method is Lutetian and is recorded by a basaltic lava flow (TER1 ≥ 45.21 ± 0.11 Ma; Table 3; Figs. 2 and 5e, f) from the Lessini Mts. The basanitic neck of the same district records a quite younger age (BOL1 ≥ 38.73 ± 0.44 Ma; Bartonian; Table 3; Figs. 2 and 5g, h) consistent with its stratigraphic position, cutting the lava flow from which TER1 was collected. The Val d'Adige district records $^{40}Ar/^{39}Ar$ ages similar to those obtained for the Lessini Mts. In particular, at Monte Baldo the lava flow (BAL1) and the sill (BAL7) record ages of 41.69 ± 0.37 Ma and 41.98 ± 0.20 Ma, respectively while the basanitic neck near Rovereto (BI14) shows an age of 40.73 ± 0.48 Ma (Tables 3 and 4; Figs. 5a–d and 6a, b). These ages are consistent with biostratigraphic ages for the interbedded carbonates (Fig. 2).

All analysed basic to acid Euganean Hills samples yielded indistinguishable ages pointing to a main magmatic phase in this district at ~32.21 ± 0.09 Ma (average value). In particular, for the basaltic trachyandesite sample (EU52) both amphibole and plagioclase separates were analysed and the resulting plateau ages are similar (32.35 ± 0.09 Ma and 32.16 ± 0.06 Ma, respectively; Table 3; Fig. 5j, l). The slight difference between the two ages for this sample may be tentatively attributed to the different closure temperatures of these two minerals, i.e., ~550 °C for hornblende and ~300 °C plagioclase. This would suggest a relatively slow cooling rate (≥1.3 °C/Ka) for the EU52 sub-intrusive body. This relatively slow cooling rate of the magma is easily understandable if we consider that EU52 intruded other basic intrusive units, which were probably nearly synchronous and thus still hot. These host basic units are geochemically equivalent to the tholeiitic basaltic products of the Euganean Hills, while EU52 is representative of the basic alkaline products of this district. The plateau age of EU52 overlaps that of the other dated Euganean basaltic trachyandesite (EU8B = 32.17 ± 0.32 Ma; Table 3; Fig. 5n). The plateau ages for the latitic, trachytic, and rhyolitic Euganean samples range between 32.09 ± 0.29 and 32.34 ± 0.51 Ma (Table 3; Fig. 5p, r, t, v). Therefore, according to the new geochronological data the peak phase of both basaltic and acidic Euganean magmatism occurred during the Rupelian (lower Oligocene; Fig. 2) in a time-span possibly shorter than 0.3 My.

Finally, both the Marosticano samples, collected in Monte Gloso quarry, point to an Aquitanian (early Miocene; ~22 Ma) eruption age (Table 3; Figs. 2, 5w, x and 6c, d). According to biostratigraphic studies and field evidences, no eruptions occurred during the Miocene neither in the Val d'Adige nor in the Euganean Hills. Therefore, the Miocene magmatic products of the eastern Lessini Mts. indicated by biostratigraphic data (Savelli and Lipparini, 1979; Fig. 2) and those of the Marosticano district represent the most recent known magmatic activity in the VVP.

The evidence for several VVP magmatic pulses reflects the main extensional phases of the southernmost portion of the Eastern Alps, which were intermitted by episodic accretionary events of the Alpine orogen (Rosenbaum and Lister, 2005). The decompressional melting of the upwelling mantle during extension of continental lithosphere is known as viable mechanism for intraplate magmatism (Pedersen and Ro, 1992). In the Paleocene (65–55 Ma) the Adria–Europe convergence stopped after the continental collision in the Eastern Alps and the following reprise of the convergence was slower than the rollback of the subducting European slab (Stampfli et al., 1998, 2002; Rosenbaum et al., 2002; Dézes et al., 2004; Schmid et al., 2004; Rosenbaum and Lister, 2005). The extension in the overriding plate is promoted when slow convergence rates do not exceed the rates of subduction rollback (Pacanovsky et al., 1999; Jolivet and Faccenna, 2000; Rosenbaum et al., 2002; Heuret and Lallemand, 2005; Rosenbaum and Lister, 2005; Brenna et al., 2015). Therefore, from the Paleocene to the middle Eocene, an extensional regime developed in the Southeastern Alps (Ratschbacher et al., 1989), triggering the magmatism in the Val d'Adige (Luciani, 1989; De Vecchi and Sedea, 1995) and in the Lessini Mts. (Borsi et al., 1969; Savelli and Lipparini, 1979; Luciani, 1989; De Vecchi and Sedea, 1995; Bassi et al., 2008) along the transtensional fault systems of the Alpone–Agno Graben (Zampieri, 1995). From the late Eocene until ~ 30 Ma an extensional regime developed in the easternmost VVP parts triggering magmatism also in the Euganean Hills (Piccoli et al., 1976, 1981; Zantendeschi, 1994; Milani et al., 1999; Bartoli et al., 2014) and Marosticano (Savelli and Lipparini, 1979). From ~30 Ma to ~23 Ma (Oligocene–Miocene boundary) the extensional processes stopped in the Southeastern Alps (Frisch et al., 2000). The magmatic activity reprised in the early Miocene, but it was quite rare and limited to the easternmost areas. No magmatic activity younger than ~ 23–20 Ma is documented (Savelli and Lipparini, 1979).

10.3. Geodynamic implications of the magmatism in the VVP

According to the new age determinations, the VVP magmatism ranges from 45.21 ± 0.11 Ma (TER1, Lessini Mts. district) to ~ 23–22 Ma (LB1 and 25B, Marosticano district). If we consider also the biostratigraphic evidence for early subacqueous volcanic activity in the Val d'Adige and the Lessini Mts., the VVP magmatism probably started from the late Paleocene (Luciani, 1989; De Vecchi and Sedea, 1995; Bassi et al., 2008). Magmatism in the Central Alps started slightly later, in the Eocene along the Periadriatic/Insubric Line, with the emplacement of the Adamello batholith and its feeder dykes at ~43 Ma (Schaltegger et al., 2009, 2019; Bergomi et al., 2015). However, the climax of the Periadriatic Central Alps orogenic magmatism occurred from 34 Ma to 28 Ma (Bergomi et al., 2015, and reference therein), during the Oligocenic extensional phase that characterized both the Central and the Eastern Alpine domains (Ring, 1994; Nievergelt et al., 1996; Challandes et al., 2003; Glodny et al., 2008; Pleuger et al., 2008; Steck, 2008; Beltrando et al., 2010; Ring and Gerdens, 2016; Schmid et al., 2017).

Despite the geographic proximity (Fig. 1a) and despite similar emplacement ages (Fig. 2), the Periadriatic Central Alps intrusive bodies and the VVP magmatic products are characterized by quite different geochemical signatures (Fig. 4a, b). The first one is characterized by sub-alkaline and calc-alkaline affinities, exhibiting trace element features typical of subduction-related magmas (high LILE/HFSE, high LREE/HFSE ratios, and low-Nb contents; Bellieni, 1980; Bellieni et al., 2010; Bergomi et al., 2015). In particular, the enrichments in LILE, Th, and U of the least evolved Periadriatic Central Alps calc-alkaline and sub-alkaline dykes (MgO > 6 wt% and mg# > 60; Fig. 4b), may result from a mantle source contaminated by subducted and recycled continental material, probably the crystalline basement of the Central Southern Alps (Bergomi et al., 2015). Contrarily, the VVP magmas span dominant alkaline to rare sub-alkaline compositions including ultrabasic, basic, intermediate, and acid rocks (Fig. 3), with the least evolved magmatic products exhibiting trace element signature typical of intraplate magmas (e.g., high HFSE contents, high LREE/HREE ratios, and relatively low LILE/HFSE ratios; Fig. 4b). In Fig. 8 the Periadriatic Central Alps magmatic products show Nb/La values significantly lower than those of VVP magmatic products (0.14–0.45 vs. 0.78–2.08, respectively), confirming a mantle source with an arc affinity for the Periadriatic Central Alps magmatism and a mantle source with an intraplate affinity for the Southeastern Alps.

Despite the clearly different geochemical compositions of the Periadriatic Central Alps and VVP magmatism, both events were

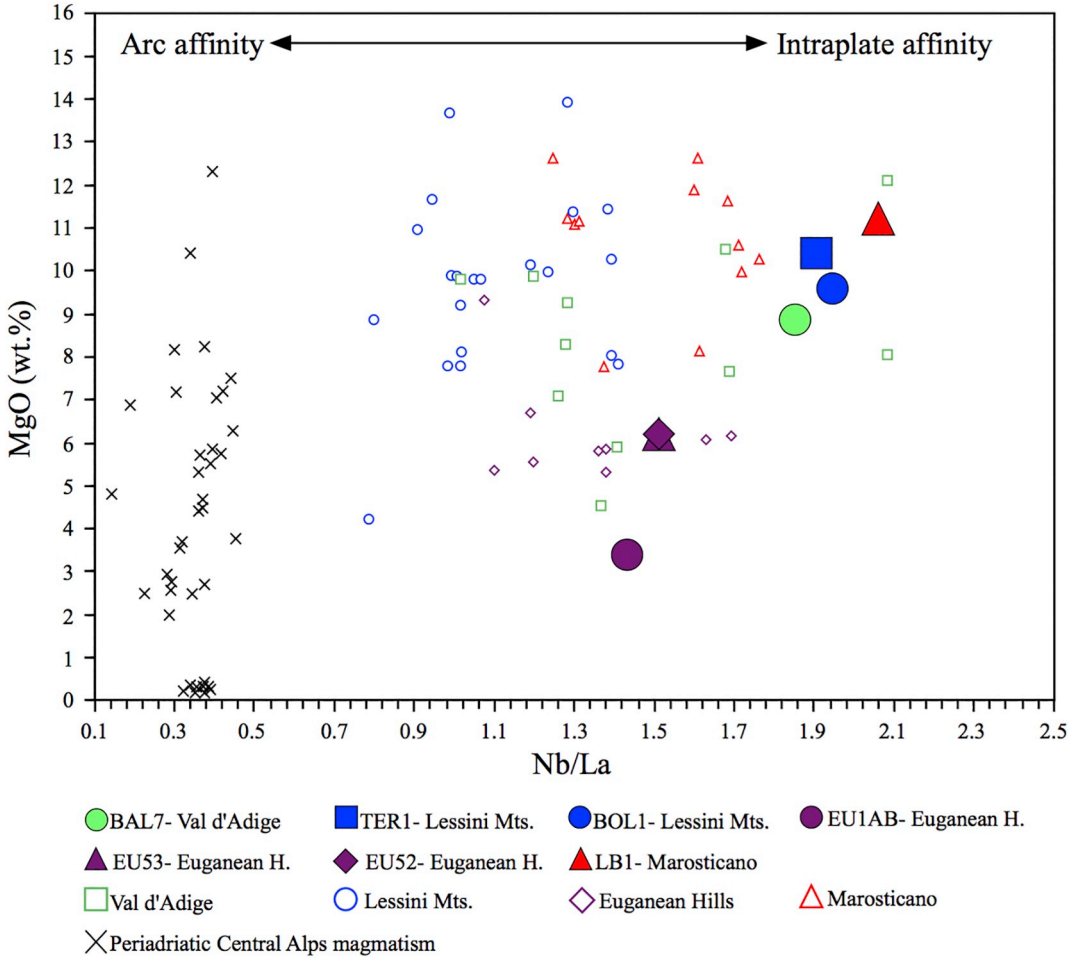

Fig. 8. MgO (wt%) vs. Nb/La diagram showing arc and intraplate affinities of mantle sources for Val d'Adige, Lessini Mts., Euganean Hills, and Marosticano rocks of this work (large solid symbols) and of previous studies (small open symbols): Val d'Adige samples are from Beccaluva et al. (2007); Lessini Mts. and Marosticano samples are from Macera et al. (2003) and Beccaluva et al. (2007); Euganean Hills samples are from Macera et al. (2003) and Milani et al. (1999). Orogenic calc-alkaline and sub-alkaline magmas of the Periadriatic Central Alps magmatism (small "x") are also reported for comparison (Bergomi et al., 2015).

explained by the slab break-off model by several authors (e.g., Davies and von Blanckenburg, 1995; von Blanckenburg and Davies, 1995; Dal Piaz et al., 2003; Macera et al., 2003; Handy et al., 2010, 2015; Bergomi et al., 2015). According to this model, at ~ 35 Ma, after the Adria–Europe collision in the Western Alps, the subducting oceanic slab detached from the European margin (Stampfli et al., 1998, 2002; Dézes et al., 2004). The break-off of the subducting slab allowed asthenospheric upwelling above the supra-subduction hydrated mantle wedge, causing its melting. However, the biostratigraphic ages suggest that the Cenozoic magmatism in the VVP started in the late Paleocene and also our new radioisotopic ages confirm that the peak activity in the Val d'Adige and the Lessini Mts. was Eocene in age (~ 45–38 Ma), well before the supposed slab break-off event. Macera et al. (2003) justified these early VVP eruptions as the result of a rising deep mantle diapir. On the contrary, Bergomi et al. (2015) proposed a partial melting of supra-subduction mantle wedge in the VVP area in response to the low-angle Alpine subduction that shifted the magmatism into the foreland. According to the latter authors, the Alpine magmatism moved then towards W–NW since the Eocene, following the steepening and retreat of the Tethyan slab, until the slab break-off in the Oligocene, which triggered the climax of the Periadriatic and VVP magmatisms.

The occurrence of low seismic velocity anomalies under the Alpine domain observed on tomographic images has been proposed as evidence for such slab detachment (e.g., Lippitsch et al., 2003; Macera et al., 2003; Piromallo and Morelli, 2003; Piromallo and Faccenna, 2004; Giacomuzzi et al., 2011; Zhao et al., 2016). However, the tomographic images themselves indicate different positions for the slab gap. Piromallo and Morelli (2003) and Piromallo and Faccenna (2004) located the slab window beneath the Central Alps, conversaly, Lippitsch et al. (2003) identified the slab detachment only below the Western Alps. Therefore, in this work we rely mainly on the recent high-resolution P-wave isotropic tomography performed by Zhao et al. (2016) and on the first P-wave anisotropic tomography (based on the induced-mantle flow orientation of olivine crystals) performed in the Alps by Hua et al. (2017). These authors used a higher number of seismic stations than the previous studies, improving the resolution of the images, essential for the interpretation of the continuity of the slab. The tomographic images of Zhao et al. (2016) and Hua et al. (2017) document a continuous European slab beneath the Central Alps without evidence of any gaps down to ~ 500 km in depth, thus ruling out the hypothesis of the slab break-off as a viable mechanism for the Cenozoic magmatism in the Alps. In particular, the length of the subducted slab in the Central Alps ranges from 450 to 500 km (Hua et al., 2017) is in accordance with the estimation of the length of a hypothetical continuous subducting slab below the Central Alps (Piromallo and Faccenna, 2004; Handy et al., 2010). Within this framework, our geochronological results and geochemical models provide constraints on the mechanisms that contributed to generate the VVP. Since the continental collision in the Eastern Alps (65 Ma), the European slab became not only progressively steeper, but also retreated in response to rollback mechanisms (Stampfli et al., 1998, 2002; Rosenbaum et al., 2002; Dézes et al., 2004; Schmid et al., 2004; Rosenbaum and Lister, 2005; Singer et al., 2014;

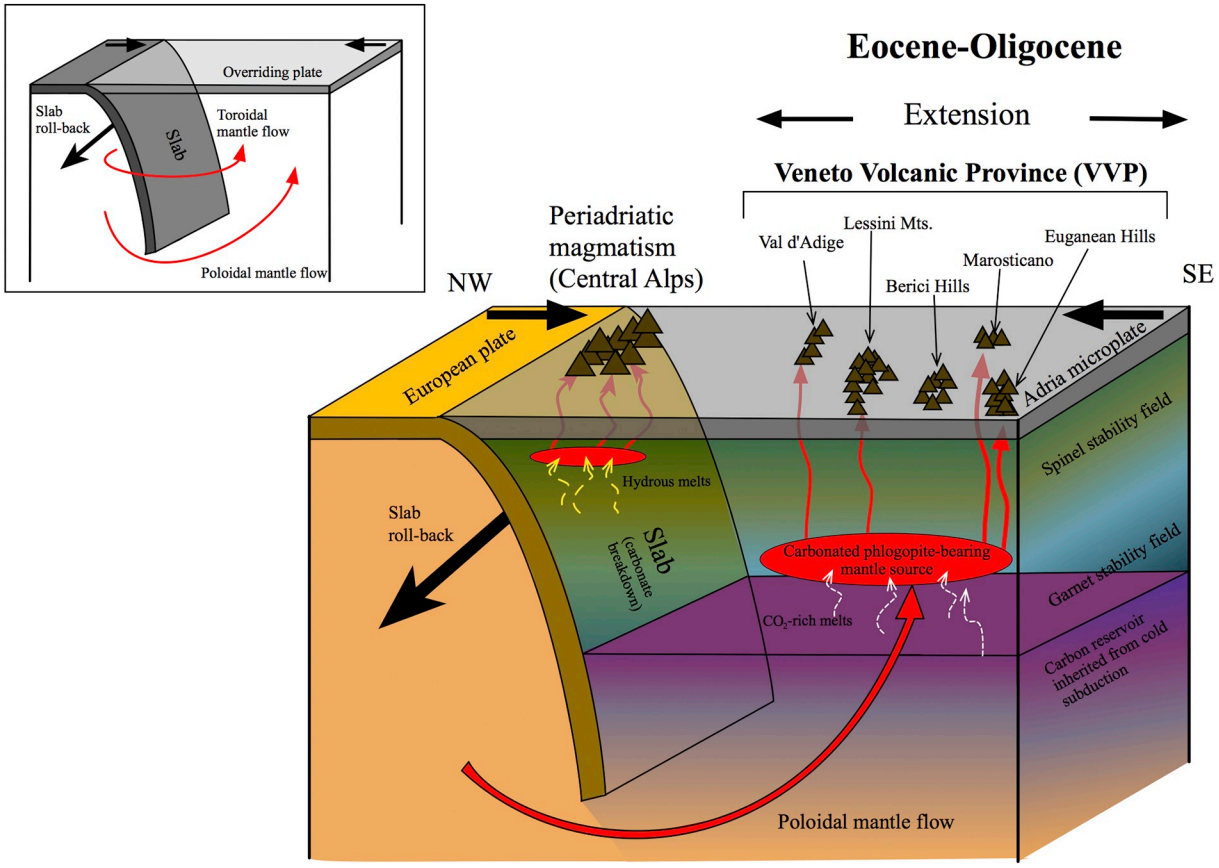

Fig. 9. Schematic model (not in scale) for the magmatism in the Central and Southeastern Alpine domains at Eocene/Oligocene. The slab rollback and steepening of the European slab induced the upwelling of a poloidal mantle flow, which causes (i) the breakdown of carbonates in calcareous metasediments and carbonated metabasics dragged at depth by the subducting slab (i.e., Malusà et al., 2018; purple zone); (ii) extensional deformation within the Adria microplate, and (iii) melting of the carbonated phlogopite-bearing garnet peridotite source, which generated the VVP magmas. In turn, the dehydration of the subducting oceanic slab induced partial melting of the overlying spinel-bearing mantle wedge, which triggered the Periadriatic orogenic magmatism.

Bergomi et al., 2015; Schlunegger and Kissling, 2015; Kissling and Schlunegger, 2018). Laboratory analogue solutions, 3D experiments, and numerical models show that the rollback subduction generates a complex mantle circulation pattern characterized by the presence of poloidal and toroidal mantle flows which escape from beneath the slab and upwelling from the tip and the lateral edges of the sinking plate, respectively (Fig. 9a; Kincaid and Griffiths, 2003; Funiciello et al., 2006; Piromallo et al., 2006; Faccenna et al., 2011; Strak and Schellart, 2014). The poloidal mantle flow can affect areas located far away from the trench, while the toroidal flow produces upwellings located only slightly laterally away from the sub-slab domain (Fig. 9a; Strak and Schellart, 2014). Both subduction-induced mantle flows (i) drive deformation, mainly extensional, in the overriding plate (Chen et al., 2016) and (ii) trigger volcanism induced by decompressional melting (Faccenna et al., 2011). We speculate that within the Alpine geological setting, the progressive retreat of the European slab caused upwelling of subduction-induced mantle flows, and in particular the poloidal mantle flow was responsible for the magmatism occurred in the VVP, well far away from the trench (Fig. 9). The circulation of this poloidal mantle flow would produce the rise of the temperature at the slab interface, causing the breakdown of the subducted carbonates stored at depth > 180 km. Then, the CO_2-rich melts metasomatised the overlying mantle lithosphere or the mantle wedge. The mantle flow upwelling reasonably induced also extensional deformation in the overriding plate and decompressional melting of the phlogopite-bearing garnet lherzolite metasomatised by CO_2-rich melts. This process triggered magmatism with intraplate signature instead of arc affinity (Fig. 9). The VVP magmatism occurred during Paleocene–Eocene in the westernmost districts (i.e., Val d'Adige-Lessini Mts. domain) and only since the Oligocene in its eastern areas (i.e., Euganean Hills-Marosticano domain). The southeastward migration and rejuvenation of the magmatism can be accounted for considering that Adria microplate underwent counterclockwise rotation of the order of 40–50° since ~ 35 Ma (Lowrie and Alvarez, 1975; Dewey et al., 1989; Rosenbaum et al., 2002; Ring and Gerdens, 2016). Such movement could have controlled the asthenospheric upwelling in different portions of the overlying lithosphere. The VVP magmatic activity went on intermittently until the early Miocene time (i.e., ~23–20 Ma; Fig. 2), when the indentation of the Adria lithosphere and the subsequent northward subduction of the Adria slab began in the Eastern Alps (Handy et al., 2015; Fig. 2). This new geodynamic configuration probably obstructed the upwelling of the poloidal mantle flow and stopped the VVP volcanic activity.

In our interpretation we rule out a passive upwelling of mantle flow through slab window(s) to explain the occurrence of the VVP magmatism. Although this was not the aim of this work, in the frame of the geodynamic model we also speculate that the Periadriatic orogenic magmatism in Central Alps is related to the dehydration of the subducting oceanic slab, which triggered the partial melting of the overlying spinel-bearing mantle wedge (Fig. 9).

10.4. Comparison with magmatism from similar geodynamic context worldwide

In several other regions worldwide, volcanism with geochemical intraplate signature occurs in proximity to subduction zones. One

possible and widely proposed interpretation of such magmatism is that it results from a mantle upwelling with a poloidal-like component induced by the rollback of a slab. A similar scenario was proposed by Kay et al. (2006, 2013) and Pallares et al. (2016) for the Payenia Volcanic Province (Argentina), a Plio–Quaternary intraplate volcanic district located close to the subduction-related Southern Volcanic Zone of the Andes. In this area the occurrence of basic and acidic rocks with OIB signature was explained by invoking an injection of asthenosphere triggered by the steepening of the subducting Nazca plate. Similarly, Faccenna et al. (2010) explained the occurrence of intraplate basaltic and silicic eruptions of the last 20 Ma in the Yellowstone Hotspot Track near the Juan de Fuca subduction system, as the result of the subduction of Juan de Fuca plate beneath the North American Plate. These authors interpreted also the intraplate French Massif Central basaltic magmatism as resulting from poloidal-like mantle flow dislodged by the retreating Calabrian slab, which accomodates the convergence between Africa and Eurasia. The main eruptions in the Massif Central occurred at 20–15 Ma and 12–1 Ma, coinciding with the opening of two back-arc basins (Liguro-Provencal and Tyrrhenian, respectively; Faccenna et al., 2010, and references therein). In this case, the poloidal-like mantle flow affected areas located at 800 km away from the trench. Brenna et al. (2012, 2015) also invoked a mantle upwelling triggered by a distal subduction to explain the magmatic activity in Jeju Island volcanic field (Korea). Here, small volumes of recent (1.8 Ma–1Ka) OIB type magmas erupted ~ 650 km away from the southwestern Japan subduction zone, where the subduction of the Philippine Sea Plate induced the upwelling of mantle flow (however, for constrating interpretations of the Korean magmatism see Tang et al., 2014; Kimura et al., 2018). An other anologue geodynamic scenario was proposed by Ferrari et al. (2001) and Neumann et al. (2016) to explain the presence of intraplate alkaline basalts near silicic and basic rocks with potassic alkaline and calc-alkaline affinities in the western Trans–Mexican volcanic belt. Here, two independent oceanic plates, Cocos and Rivera, converge against the North American Plate. According to Ferrari et al. (2001), the sinking of the Rivera slab may have induced small amounts of asthenosphere to flow laterally into the mantle wedge generating the intraplate volcanism. However, the origin of this magmatism is still debated. For example, Gómez-Tuena et al. (2011, 2018) proposed that the coexistence of magmatic rocks with subduction and intraplate signatures is due to different chemical input released from the slab at different thermal conditions.

Inset a) Sketch showing poloidal and toroidal mantle flow geometries. The poloidal mantle flow escapes from beneath the slab and upwells from its tip, affecting mantle region(s) located far away from the sinking plate (the VVP case); the toroidal flow escapes from the lateral edges of the slab and upwells only in the mantle portion(s) near the slab. (For interpretation of the references to colour in this figure legend, the reader is referred to the web version of this article.)

11. Conclusion

The intraplate magmatism of the VVP region occurred in an extensional setting at the same time of the Alpine orogeny. The VVP basic–ultrabasic magmatic products (alkaline to tholeiitic in composition) exhibit enrichments in Ba, Sr, and P, and depletions in Zr, Hf, and Ti. This suggests a provenance for a variable metasomatised mantle source. According to geochemical modelling, these magmas formed by ~ 1.5–4% degrees of partial melting of a carbonated phlogopite-bearing garnet peridotite mantle source. The “carbonatitic” metasomatic agent of the VVP mantle source was possibly derived by the breakdown of carbonates in calcareous metasediments and carbonated metabasics dragged at depth by the subducting Tethys slab.

By integrating literature biostratigraphic data with new $^{40}Ar/^{39}Ar$ geochronological data for the VVP, we reconstructed the temporal evolution of the magmatic activity of this province. The first magmatic activities occurred in the westernmost VVP domain (i.e., Val d'Adige and Lessini Mts.) during the Paleocene–Eocene when an extensional regime was imposed in the Southeastern Alps by the rollback of the subducted oceanic slab. During the Oligocene–Miocene another extensional phase occurred promoting magmatism also in the easternmost VVP domain (i.e., Euganean Hills and Marosticano district). According to this reconstruction the first VVP eruptions are pre–Oligocene in age, ruling out the hypothesis that the magmatism was due to the upwelling of mantle diapirs through a slab window after the European slab detachment, which occurrence was dated after ~ 35 Ma. Moreover, in accordance with recently published tomographic images, the present European slab is continuous and nearly vertical, with a tip at ~ 500 km in depth. Thus, a new geodynamic model is here proposed:

- the progressive retreatment and steepness of the European slab induced the escape of the sub-slab mantle material and its upwelling mainly from the front of the slab;
- the subduction-induced mantle flow caused heating at the slab interface and, by consequence, breakdown of carbonates and generation of metasomatising CO_2-rich melts;
- the upwelling of the mantle flow triggered the intraplate magmatism in the Alpine collisional setting driving localized extensional deformation in Adria microplate and decompression melting of the metasomatised mantle beneath the VVP.

Finally, we also speculate that the southeastward migration and rejuvenation of the magmatism is an effect counterclockwise rotation of Adria microplate, which started at ~ 35 Ma. In addition, we suggest that the coeval Periadriatic orogenic magmatism occurred in the Central Alps is related to the partial melting of the spinel-bearing mantle wedge induced by dehydration of the subducting slab.

Acknowledgments

We thank Renzo Tassinari (University of Ferrara) and Daria Pasqual (University of Padova) for ICP–MS and XRF analyses respectively; Roberto Zorzin for field-work and logistical contributions; Adam Frew and Celia Mayers (WAAIF), and Dan Jones (University of Vermont) for assistance during sample preparation and geochronological analyses.

The critical and constructive reviews of M. Brenna and an anonymous referee as well as the thoughtful editorial handling of Arturo Gómez-Tuena helped to substantially improve an early version of this work.

Funding

V. Brombin was funded by IUSS Mobility Research Programme (VB scholarship for Abroad Mobility for Long Period 04/11/2015) and Young Researcher Grant of the University of Ferrara (Italy) (Pr. No. 101908). Field and laboratory work for this project were supported by the Museo Civico di Storia Naturale di Verona and Regione Veneto. C. Bonadiman and A. Marzoli were funded by the Italian Government PRIN 2015–2016 (Pr. No. 20158A9CBM) and PRIN 2017-2018 (Pr. No. 20178LPCPW) funds.

Appendix A. Supplementary data

Supplementary data to this article can be found online at https://doi.org/10.1016/j.earscirev.2019.03.016.

References

Alagna, K.E., Peccerillo, A., Martin, S., 2010. Tertiary to present evolution of Orogenic magmatism, in Italy. J. Virtual Explor. 36 (paper 18, in: Beltrando, M., Peccerillo, A., Mattei, M., Conticelli, S., Doglioni C., (Eds.), The Geology of Italy: Tectonics and Life Along Plate Margins).

Aldanmaz, E., Köprübaşi, N., Gürer, Ö.F., Kaymakçi, N., Gourgand, A., 2006. Geochemical constraints on the Cenozoic, OIB-type alkaline volcanic rocks of NW Turkey:

implications for mantle sources and melting processes. Lithos 86, 50–76. https://doi.org/10.1016/j.lithos.2005.04.003.
Allan, J.F., Nelson, S.A., Luhr, J.F., Carmichael, I.S.E., Wopat, M., Wallace, P., 1991. Pliocenerecent rifting in SW Mexico and associated volcanism: an exotic terrain in the making. In: Dauphin, J.P., Simoneit, B.R.T. (Eds.), The Gulf and Peninsular Province of the Californias. 47. pp. 425–445 (AAPG Memoir).
Allen, M.B., Kheirkhah, M., Neill, I., Emami, M.H., McLeod, C.L., 2013. Generation of arc and within-plate chemical signatures in collision zone magmatism: Quaternary lavas feom Kurdistan Province. Iran. J. Petrol. 54, 887–911. https://doi.org/10.1093/petrology/egs090.
Aragón, E., Pinotti, L., D'Eramo, F., Castro, A., Rabbia, O., Coniglio, J., Demartis, M., Hernando, I., Cavarozzi, C.E., Aguilera, Y.E., 2013. The Farallon-Aluk ridge collision with South America: implications for the geochemical changes of slab window magmas from fore- to back-arc. Geosci. Front. 4, 377–388. https://doi.org/10.1016/j.gsf.2012.12.004.
Aulbach, S., Griffin, W.L., O'Reilly, S.Y., McCandless, T.E., 2004. Genesis and evolution of the lithospheric mantle beneath the Buffalo Head Terrane, Alberta (Canada). Lithos 77, 413–451. https://doi.org/10.1016/j.lithos.2004.04.020.
Baksi, A.K., 2006. Guidelines for assessing the reliability of $^{40}Ar/^{39}Ar$ plateau ages: application to ages relevant to hotspot tracks. http://www.mantleplumes.org/ArAr.html.
Barbieri, G., Medizza, F., 1969. Contributo alla conoscenza geologica della regione di Bolca (Monti Lessini). Mem. Ist. Geol. Min. Univ. Pad. 27, 1–36.
Barbieri, G., De Zanche, V., Sedea, R., 1991. Evoluzione del semigraben paleogenico Alpone–Agno (Monti Lessini). Rend. Soc. Geol. Ital. 14, 5–12.
Bartoli, O., Meli, S., Bergomi, M.A., Sassi, R., Magaraci, D., Liu, D.Y., 2014. Geochemistry and zircon U–Pb geochronology of magmatic enclaves in trachytes from the Euganean Hills (NE Italy): further constraints on Oligocene magmatism in the eastern Southern Alps. Eur. J. Mineral. 27, 161–174. https://doi.org/10.1127/ejm/2015/0027–2425.
Bassi, D., Bianchini, G., Mietto, P., Nebelsick, J.H., 2008. Southern Alps: Venetian Pre-Alps. In: McCann, T. (Ed.), The Geology of Central Europe, 2, pp. 1087–1092 Geol. Soc. London.
Beccaluva, L., Bonadiman, C., Coltorti, M., Salvini, L., Siena, F., 2001. Depletion events, nature of metasomatizing agent and timing of enrichment processes in lithospheric mantle xenoliths from the VVP. J. Petrol. 42, 173–187. https://doi.org/10.1093/petrology/42.1.173.0.
Beccaluva, L., Bianchini, G., Bonadiman, C., Coltorti, M., 2007. Intraplate lithospheric and sublithospheric components in the Adriatic domain: Nephelinite to tholeiite magma generation in the Paleogene Veneto Volcanic Province, Southern Alps. Geol. Soc. Am. 418, 131–152. https://doi.org/10.1130/2007.2418(07).
Begemann, F., Ludwig, K.R., Lugmair, G.W., Min, K., Nyquisit, L.E., Patchett, P.J., Renne, P.R., Shih, C.Y., Villa, I.M., Walker, R.J., 2001. Call for an improved set of decay constants for geochronological use. Geochim. Cosmochim. Acta 65, 111–121. https://doi.org/10.1016/S0016–7037(00)00512–3.
Bellieni, G., 1980. The Cima di Villa (Zinsnock) massif: geochemical features and comparisons with the Vedrette di Ries (Rieserferner) pluton (Eastern Alps, Italy). Neues Jb. Mineral. Abh. 138, 244–258.
Bellieni, G., Fioretti, A.M., Marzoli, A., Visonà, D., 2010. Permo–Paleogene magmtism in the eastern Alps. Rend. Fis. Acc. Lincei 21, 51–71. https://doi.org/10.1007/s12210-010-0095-z.
Beltrando, M., Lister, G.S., Rosenbaum, G., Richards, S., Forster, M.A., 2010. Recognizing episodic lithospheric thinning along a convergent plate margin: the example of the Early Oligocene Alps. Earth Sci. Rev. 103, 81–98. https://doi.org/10.1016/j.earscirev.2010.09.001.
Bergomi, M.A., Zanchetta, S., Tunesi, A., 2015. The Tertiary dike magmaism in the Southern Alps: geochronological data and geodynamic significance. Int. J. Earth Sci. 104, 449–473. https://doi.org/10.1007/s00531–014–1087–5.
Bogaard, P.J.F., Wörner, G., 2003. Petrogenesis of basanitic to tholeiitic volcanic rocks from the Miocene Vogelsberg, Central Germany. J. Petrol. 44, 569–602. https://doi.org/10.1093/petrology/44.3.569.
Borsi, S., Ferrara, G., Piccoli, G., 1969. Determinazioni col metodo K/Ar dell'età delle eruzioni euganee. Rend. Soc. Ital. Mineral. Petrol. 25, 27–34.
Brack, P., 1981. Structures in the southwestern border of the Adamello intrusion. Swiss Bull. Mineral. Petrol. 61, 37–50. https://doi.org/10.5169/seals–47129.
Brack, P., 1984. Geologie der Intrusiva und Nebengesteine des Südwest–Adamello (Nord–Italien). Ph.D. thesis, Dissertation ETH. Nr. 7612.
Bradley, D.C., Kusky, T., Heaussler, P.J., Goldfarb, R.J., Miller, M.L., Dumuolin, J.A., Nelson, S.W., Karl, S.M., 2003. Geological signature of early Tertiary ridge subduction in Alaska. Geol. Soc. Am. Spec. 371, 19–49. https://doi.org/10.1130/0–8137–2371–X.19.
Brenna, M., Cronin, S.J., Smith, I.E.M., Maas, R., Sohn, Y.K., 2012. How small-volume basaltic magmatic systems develop: a case study from the Jeju Island Volcanic Field, Korea. J. Petrol. 53, 985–1018. https://doi.org/10.1093/petrology/egs007.
Brenna, M., Cronin, S.J., Kereszturi, G., Sohn, Y.K., Smith, I.E.M., Wijbrans, J., 2015. Intraplate volcanism influenced by distal subduction tectonics at Jeju Island, Republic of Korea. Bull. Volcanol. 77, 1–16. https://doi.org/10.1007/s00445–014–0896–5.
Briggs, R.M., McDonough, W.F., 1990. Contemporaneous convergent margin and intraplate magmatism, North Island, New Zealand. J. Petrol. 31, 813–851. https://doi.org/10.1093/petrology/31.4.813.
Brombin, V., Bonadiman, C., Coltorti, M., Fahnestock, M.F., Bryce, J.G., Marzoli, A., 2018. Refertilized mantle keel below the Southern Alps domain (North–East Italy): evidence from Marosticano refractory mantle peridotites. Lithos 300–301, 72–85. https://doi.org/10.1016/j.lithos.2017.11.032.
Callegari, E., Brack, P., 2002. Geological map of the Tertiary Adamello batholith (Northern Italy). Explanatory notes and legend. Mem. Sci. Geol. 54, 19–49.
Carminati, E., Doglioni, C., 2012. Alps vs. Appennines: the paradigm of a tectonically asymmetric Earth. Earth Sci. Rev. 112, 67–96. https://doi.org/10.1016/j.earscirev.2012.02.004.
Carminati, E., Wortel, M.J.R., Spakman, W., Sabadini, R., 1998. The role of slab detachment processes in the opening of the western-Central Mediterranean basins: some geological and geophysical evidence. Earth Planet. Sci. Lett. 160, 651–665. https://doi.org/10.1016/S0012-821X(98)00118-6.
Challandes, N., Marquer, D., Villa, I.M., 2003. Dating the evolution of C–S microstructures: a combined $^{40}Ar/^{39}Ar$ step-heating and UV laserprobe analysis of the Alpine Roffna shear zone. Chem. Geol. 197, 3–19. https://doi.org/10.1016/S0009–2541(02)00354–6.
Chen, Z., Schellart, W.P., Strak, V., Duarte, J.C., 2016. Does subduction-induced mantle flow drive back–arc subduction? Earth Planet. Sci. Lett. 441, 200–210. https://doi.org/10.1016/j.epsl.2016.02.027.
Coltorti, M., Bonadiman, C., Faccini, B., Piromallo, C., 2009. Constraints on mantle flow in subduction system as inferred from petrological features of magmas and mantle xenoliths. In: "From Core to Crust: Towards an Integrated Vision of Earth's Interior" ICTP, Trieste, 20–24 July 2009.
Conticelli, S., Guarnieri, L., Farinelli, A., Mattei, M., Avanzinelli, R., Bianchini, G., Boari, E., Tommasini, S., Tiepolo, M., Prelevic, D., Venturelli, G., 2009. Trace-elements and Sr–Nd–Pb isotopes of K–rich, shoshonitic, and calc-alkaline magmatism of the Western Mediterranean region: genesis of ultrapotassic to calcalkaline magmatic association in a post–collisional geodynamic setting. Lithos 107, 69–92. https://doi.org/10.1016/j.lithos.2008.07.016.
Cook, C., Briggs, R.M., Smith, I.E.M., Maas, R., 2005. Petrology and geochemistry of intraplate basalts in the South Auckland Volcanic Filed, New Zealand: evidence for two coeval magma suites from distinct sources. J. Petrol. 46, 473–503. https://doi.org/10.1093/petrology/egh084.
Dal Piaz, G.V., Bistacchi, A., Massironi, M., 2003. Geological outline of the Alps. Episodes 26, 175–181.
Dal Zilio, L., Faccenda, M., Capitanio, F., 2018. The role of deep subduction in supercontinent breakup. Tectonophysics 746, 312–324. https://doi.org/10.1016/j.tecto.2017.03.006.
Davies, J.H., von Blanckenburg, F., 1995. Slab breakoff: a model of lithosphere detachment and its test in the magmatism and deformation of collisional orogens. Earth Planet. Sci. Lett. 129, 85–102. https://doi.org/10.1016/0012-821X(94)00237-S.
de Boer, J.Z., Defant, M.J., Stewart, R.H., Restrepo, J.P., Clark, L.F., Ramirez, A.H., 1988. Quaternary calc-alkaline volcanism in western Panama: regional variation and implication for the plate tectonic framework. J. S. Am. Earth Sci. 1, 275–293. https://doi.org/10.1016/0895–9811(88)90006–5.
De Vecchi, G., Sedea, R., 1995. The Paleogene basalts of the Veneto region (NE Italy). Mem. Sci. Geol. 47, 253–374.
De Vecchi, G., Gregnanin, A., Piccirillo, E.M., 1976. Aspetti petrogenetici del vulcanesimo terziario Veneto. Mem. Ist. Geol. Min. Univ. Pad. 30, 1–63.
Deng, L., Liu, Y., Zong, K., Zhu, L., Xu, R., Hu, Z., Gao, S., 2017. Trace element and Sr isotope records of multi-episode carbonatite metasomatism on the eastern margin of the North China Craton. Geochem. Geophys. Geosyst. 18, 220–237. https://doi.org/10.1002/2016GC006618.
Dewey, J.F., Helman, M.L., Turco, E., Hutton, D.H.W., Knott, S.D., 1989. Kinematics of the western Mediterranean, in Alpine Tectonics. Geol. Soc. Spec. Publ. London 45, 265–283. https://doi.org/10.1144/GSL.SP.1989.045.01.15.
Dézes, P., Schmid, S.M., Ziegler, P.A., 2004. Evolution of the European Cenozoic Rift System: interaction of the Alpine and Pyrenean orogenes with their foreland lithosphere. Tectonophysics 389, 1–33. https://doi.org/10.1016/j.tecto.2004.06.011.
Dixon, J., Clague, D.A., Cousens, B., Monsalve, M.L., Uhl, J., 2008. Carbonatite and silicate melt metasomatism of the mantle surrounding the Hawaiian plume: evidence from volatiles, trace elements, and radiogenic isotopes in rejuvenated–stage lavas from Niihau, Hawaii. Geochem. Geophys. 9. https://doi.org/10.1029/2008GC002076.
Faccenna, C., Becker, T.W., Lallemand, S., Lagabrielle, Y., Funiciello, F., Piromallo, C., 2010. Subduction-triggered magmatic pulses: a new class of plumes? Earth Planet. Sci. Lett. 299, 54–68. https://doi.org/10.1016/j.epsl.2010.08.012.
Faccenna, C., Molin, P., Orecchio, B., Olivetti, V., Bellier, O., Funiciello, F., Minelli, L., Piromallo, C., Billi, A., 2011. Topography of the Calabria subduction zone (southern Italy): clues for the origin of Mt. Etna. Tectonics 30, TC1003. https://doi.org/10.1029/2010TC002694.
Faccini, B., Coltorti, M., Bonadiman, C., 2018. Contemporaneous Emission of Calcalkaline and Alkaline Magmas in Subductive Geodynamic Settings: A Mantle Xenolith Perspective. Book of Abstracts, 3rd European Mantle Workshop – Pavia, 43.
Ferrari, L., 2004. Slab detachment control on mafic volcanic pulse and mantle heterogeneity in Central Mexico. Geology 32, 77–80. https://doi.org/10.1130/G19887.1.
Ferrari, L., Petrone, C.M., Francalanci, L., 2001. Generation of oceanic-island basalt-type volcanism in the western Trans–Mexican volcanic belt by slab rollback, asthenosphere infiltration, and variable flux melting. Geology 29, 507–510. https://doi.org/10.1130/0091–7613(2001)029<0507:GOOIBT>2.0.CO;2.
Foulger, G.R., Panza, G.F., Artemieva, I.M., Bastow, I.D., Cammarano, F., Doglioni, C., Evans, J.R., Hamilton, W.B., Julian, B.R., Lustrino, M., Thybo, H., Yanovskaya, T., 2015. What lies deep in the mantle below? EOS 96. https://doi.org/10.1029/2015EO034319.
Frascari Ritondale Spano, F., 1969. Serie Paleogeniche nell'area pedemontana a Sud dell'Altopiano di Asiago (Vicenza, Italia). Bur. Rech. Géol. Min. Mém. 69, 173–182.
Frascari Ritondale Spano, F., Bassani, P., 1973. Ricerche geologiche nei dintorni di Bassano del Grappa (Vicenza). Memorie Museo Trid. Sci. Nat. 19, 65–112.
Frezzotti, M.L., Peccerillo, A., Panza, G., 2009. Carbonate metasomatism and CO_2 lithosphere–asthenosphere degassing beneath the Western Mediterranean: an integrated

model arising from petrological and geophysical data. Chem. Geol. 262, 108–120. https://doi.org/10.1016/j.chemgeo.2009.02.015.
Frisch, W., Dunkl, I., Kuhlemann, J., 2000. Post-collisional orogen-parallel large-scale extension in the Eastern Alps. Tectnophysics 327, 239–265. https://doi.org/10.1016/S0040–1951(00)00204–3.
Frost, D.J., 2006. The stability of hydrous mantle phases. Rev. Mineral. Geochem. 62, 243–271. https://doi.org/10.2138/rmg.2006.62.11.
Frost, D.J., 2008. The upper mantle and transition zone. Elements 4, 171–176. https://doi.org/10.2113/GSELEMENTS.4.3.171.
Funiciello, F., Moroni, M., Piromallo, C., Faccenna, C., Cenedese, C., Bui, H.A., 2006. Mapping mantle flow during retreating subduction: Laboratory models analysed by feature tracking. J. Geophys. Res. 111, B03402. https://doi.org/10.1029/2005JB003792.
Furman, T., Graham, D., 1999. Erosion of lithospheric mantle beneath the East African Rift system: geochemical evidence from the Kivu volcanic province. Lithos 48, 237–262. https://doi.org/10.1016/S0024–4937(99)00031–6.
Fytikas, M., Innocenti, F., Manetti, P., Peccerillo, A., Mazzuoli, R., Villari, L., 1984. Tertiary to Quaternary evolution of volcanism in the Aegean region. Geol. Soc. Spec. Publ. London 17, 687–699. https://doi.org/10.1144/GSL.SP.1984.017.01.55.
Garzanti, E., Radeff, G., Malusà, M.G., 2018. Slab breakoff: a critical appraisal of a geological theory as applied in space and time. Earth Sci. Rev. 177, 303–319. https://doi.org/10.1016/j.earscirev.2017.11.012.
Gasperini, D., Bosch, D., Braga, R., Bondi, M., Macera, P., Morten, L., 2006. Ultramafic xenoliths from the Veneto Volcanic Province (Italy): Petrological and geochemical evidence for multiple metasomatism of the SE Alps mantle lithospere. Geochem. J. 40, 377–404. https://doi.org/10.2343/geochemj.40.377.
Gatta, G.D., McIntyre, G.J., Sassi, R., Rotiroti, N., Pavese, A., 2011. Hydrogen-bond and cation partitioning in muscovite: a single-crystal neutron-diffraction study at 295 and 20 K. Am. Mineral. 96, 34–41. https://doi.org/10.2138/am.2011.3595.
Gavioli, G., 1972. Ricerche stratigrafiche e tettoniche nei dintorni di Malo (Vicenza). Tesi di laurea, Istituto di Geologia Università di Bologna.
Giacomuzzi, G., Chiarabbia, C., De Gori, P., 2011. Linking the Alps and Apennines subduction systems: New constraints revealed by high-resolution teleseismic tomography. Earth Planet. Sci. Lett. 301, 531–543. https://doi.org/10.1016/j.epsl.2010.11.033.
Giusberti, L., Del Favero, L., Roghi, G., 2014. The Purga di Bolca-Vegroni sites. In: Papazzoni, C.A., Giusberti, L., Carnevale, G., Roghi, G., Bassi, D., Zorzin, R. (Eds.), The Bolca Fossil-Lagerstätten: A Window into the Eocene World. Rendiconti della Società Paleontologica Italiana, vol. 4. pp. 95–103.
Glodny, J., Ring, U., Kühn, A., 2008. High-pressure metamorphism, thrusting, strike-slip and extensional shearing in the Tauern Window, Eastern Alps: all starting at the same time? Tectonics 27, TC4004. https://doi.org/10.1029/2007TC002193.
Goes, S., Spakman, W., Bijwaard, H., 1999. A lower mantle source for central European volcanism. Science 286, 1928–1931. https://doi.org/10.1126/science.286.5446.1928.
Gómez-Tuena, A., Mori, L., Goldstein, S.L., Pérez-Arvizu, O., 2011. Magmatic diversity of westernMexico as a function of metamorphic transformations in the subducted oceanic plate. Geochim. Cosmochim. Acta 75, 213–241. https://doi.org/10.1016/j.gca.2010.09.029.
Gómez-Tuena, A., Mori, L., Straub, S.M., 2018. Geochemical and petrological insights into the tectonic origin of the Transmexican Volcanic Belt. Earth Sci. Rev. 183, 153–181. https://doi.org/10.1016/j.earscirev.2016.12.006.
Green, D.H., Ringwood, A.E., 1970. Mineralogy of peridotitic compositions under upper mantle conditions. Phys. Earth Planet. Inter. 3, 359–371. https://doi.org/10.1016/0031–9201(70)90076–2.
Green, D.H., Blundy, J.D., Adam, J., Yaxley, G.M., 2000. SIMS determination of trace element partition coefficients between garnet, clinopyroxene and hydrous basaltic liquids at 2–7.5 GPa and 1020–1200°C. Lithos 53, 165–187. https://doi.org/10.1016/S0024–4937(00)00023–2.
Greenough, J.D., Hayatsu, A., Papezik, V.S., 1988. Mineralogy, petrology and geochemistry of the alkaline Malpeque Bay sill, Prince Edward Island. Can. Mineral. 26, 97–108.
Handy, M.R., Schmid, S.M., Bousquet, R., Kissling, E., Bernoulli, D., 2010. Reconciling plate-tectonic reconstructions of Alpine Tethys with the geological–geophysical record of spreading and subduction in the Alps. Earth Sci. Rev. 102, 121–158. https://doi.org/10.1016/j.earscirev.2010.06.002.
Handy, M.R., Ustaszewski, K., Kissling, E., 2015. Reconstructing the Alps-Carpathians-Dinarides as a key to understanding switches in subduction polarity, slab gaps and surface motions. Int. J. Earth Sci. 104, 1–26. https://doi.org/10.1007/s00531-014-1060-3.
Harangi, S., Downes, H., Seghedi, I., 2006. Tertiary–Quaternary subduction processes and related magmatism in the Alpine–Mediterranean region. Geol. Soc. Lond. Mem. 32, 167–190. https://doi.org/10.1144/GSL.MEM.2006.032.01.10.
Hellebrand, E., Snow, J.E., Hoppe, P., Hofmann, A.W., 2002. Garnet–field melting and late–stage refertilization in "residual" abyssal peridotites from the Central Indian Ridge. J. Petrol. 43, 2305–2338. https://doi.org/10.1093/petrology/43.12.2305.
Heuret, A., Lallemand, S., 2005. Plate motions, slab dynamics and back-arc deformation. Phys. Earth Planet. Inter. 149, 31–51. https://doi.org/10.1016/j.pepi.2004.08.022.
Hoernle, K., Zhang, Y.S., Graham, D., 1995. Seismic and geochemical evidence for large-scale mantle upwelling beneath the eastern Atlantic and western and Central Europe. Nature 374, 34–39. https://doi.org/10.1038/374034a0.
Hua, Y., Zhao, D., Xu, Y., 2017. P wave anisotropic tomography of the Alps. J. Geophys. Res. Solid Earth 122, 4509–4528. https://doi.org/10.1002/2016JB013831.
Ionov, D.A., O'Reilly, S.Y., Kopylova, M.G., Genshaft, Y.S., 1996. Carbonate–bearing mantle peridotite xenoliths from Spitsbergen: phase relationships, mineral compositions and trace element residence. Contrib. Mineral. Petrol. 125, 375–392. https://doi.org/10.1007/s004100050229.
Irvine, T.N., Baragar, W.R.A., 1971. A guide to the chemical classification of the common volcanic rocks. Can. J. Earth Sci. 8, 523–548. https://doi.org/10.1139/e71–055.
Jolivet, L., Faccenna, C., 2000. Mediterranean extension and the Africa-Eurasia collision. Tectonics 19, 1095–1106. https://doi.org/10.1029/2000TC900018.
Jourdan, F., Féraud, G., Bertrand, H., Watkeys, M.K., 2007. From flood basalts to the onset of oceanization: example from the $^{40}Ar/^{39}Ar$ high-resolution picture of the Karoo large igneous province. Geochem. Geophys. 8, Q02002. https://doi.org/10.1029/2006GC001392.
Kagami, H., Ulmer, P., Hansmann, W., Dietrich, V., Steiger, R.H., 1991. Nd–Sr isotopic and geochemical characteristics of the southern Adamello (Northern Italy) intrusives: implications for crustal versus mantle origin. J. Geophys. Res. 96, 14331–14346. https://doi.org/10.1029/91JB01197.
Kay, S.M., Mancilla, O., Copeland, P., 2006. Evolution of the backarc Chachahuén volcanic complex at 37°S latitude over a transient Miocene shallow subduction zone under the Neuquén Basin. Geol. Soc. Am. Spec. Pap. 407, 215–246. https://doi.org/10.1130/2006.2407(10).
Kay, S.M., Ardolino, A.A., Gorring, M., Ramos, V., 2007. The Somuncura large igneous province in Patagônia: interaction of a transient mantle thermal anomaly with a subducting slab. J. Petrol. 48, 43–77. https://doi.org/10.1093/petrology/egl053.
Kay, S.M., Jones, H.A., Kay, R.W., 2013. Origin of Tertiary to recent EM- and subduction-like chemical and isotopic signatures in Auca Mahuida region (37°–38°S) and other Patagonian plateau lavas. Contrib. Mineral. Petrol. 166, 165–192. https://doi.org/10.1007/s00410–013–0870–9.
Kimura, J.I., Sakuyama, T., Miyazaki, T., Bogdan, S.V., Yoshio, F., Stern, R.J., 2018. Plume-stagnant slab-lithosphere interations: origin of the late Cenozoic intra-plate basalts on the East Eurasia margin. Lithos 300–301, 227–249. https://doi.org/10.1016/j.lithos.2017.12.003.
Kincaid, C., Griffiths, R.W., 2003. Laboratory models of the thermal evolution of the mantle during rollback subduction. Nature 425, 58–62. https://doi.org/10.1038/nature01923.
Kissling, E., Schlunegger, F., 2018. Rollback ororgeny model for the evolution of the Swiss Alps. Tectonics 37, 1097–1115. https://doi.org/10.1002/2017TC004762.
LaTourette, T., Hervig, R.L., Holloway, J.R., 1995. Trace element partitioning between amphibole, phlogopite, and basanite melt. Earth Planet. Sci. Lett. 135, 13–30. https://doi.org/10.1016/0012–821X(95)00146–4.
Le Maitre, R.W., Streckeisen, A., Zanettin, B., Le Bas, M.J., Bonin, B., Bateman, P., Bellieni, G., Dudek, A., Efremova, S., Keller, J., Lamere, J., Sabine, P.A., Schmid, R., Sorensen, H., Woolley, A.R., 2002. Igneous Rocks: A Classification and Glossary of Terms, Recommendations of the International Union of Geological Sciences Subcommission of the Systematics of Igneous Rocks. Cambridge University Press, UK.
Lee, J.Y., Marti, K., Severinghaus, J.P., Kawamura, K., Yoo, H.-S., Lee, J.B., Kim, J.S., 2006. A redetermination of the isotopic abundance of atmospheric Ar. Geochim. Cosmochim. Acta 70, 4507–4512. https://doi.org/10.1016/j.gca.2006.06.1563.
Lippitsch, R., Kissling, E., Ansorge, J., 2003. Upper mantle structure beneath the Alpine orogen from high–resolution teleseismic tomography. J. Geophys. Res. 108 (B8), 2376. https://doi.org/10.1029/2002JB002016.
Lowrie, W., Alvarez, W., 1975. Paleomagnetic evidence for rotation of the Italian Peninsula. J. Geophys. Res. 80, 1579–1592. https://doi.org/10.1029/JB080i011p01579.
Luciani, V., 1989. Stratigrafia sequenziale del Terziario nella Catena del Monte Baldo (Provincie di Verona e Trento). Mem. Sci. Geol. 41, 263–351.
Luhr, J.F., Nelson, S., Allan, J.F., Carmichael, I.S.E., 1985. Active rifting in southwestern Mexico: manifestations of an incipient eastward spreading-ridge jump. Geology 13, 54–57. https://doi.org/10.1130/0091-7613(1985)13<54:ARISMM>2.0.CO;2.
Lustrino, M., Wilson, M., 2007. The circum-Mediterranean anorogenic Cenozoic igneous province. Earth Sci. Rev. 81, 1–65. https://doi.org/10.1016/j.earscirev.2006.09.002.
Macera, P., Gasperini, D., Piromallo, C., Blichert-Toft, J., Bosch, D., Del Moro, A., Martin, S., 2003. Geodynamic implications of deep mantle upwelling in the source of Tertiary volcanics from the Veneto region (Southern-Eastern Alps). J. Geodyn. 36, 563–590. https://doi.org/10.1016/j.jog.2003.08.004.
Macera, P., Gasperini, D., Ranalli, G., Mahatsente, R., 2008. Slab detachment and mantle plume upwelling in subduction zones: an example from the Italian South–Eastern Alps. J. Geodyn. 45, 32–48. https://doi.org/10.1016/j.jog.2007.03.004.
Maierov, P., Schulmann, K., Gerya, T., 2018. Relamination styles in collisional orogenes. Tectonics 37, 224–250. https://doi.org/10.1002/2017TC004677.
Malusà, M.G., Frezzotti, M.L., Ferrando, S., Brandmayr, E., Romanelli, F., Panza, G.F., 2018. Active carbon sequestration in the Alpine mantle wedge and implications for long–term climate trends. Sci. Rep. 8, 1–8. https://doi.org/10.1038/s41598–018–22877–7.
Manzotti, P., Ballèvre, M., Zucali, M., Robyr, M., Engi, M., 2014. The tectonometamorphic evolution of the Sesia-Dent Blanche nappes (internal Western Alps): review and synthesis. Swiss J. Geosci. 107, 309–336. https://doi.org/10.1007/s00015–014–0172–x.
McDonough, W.F., Sun, S.S., 1995. The composition of the Earth. Chem. Geol. 120, 223–253. https://doi.org/10.1016/0009–2541(94)00140–4.
McDougall, I., Harrison, T.M., 1999. Geochronology and Thermochronology by the $^{40}Ar/^{39}Ar$ Method. Oxford University Press, New York.
Medizza, F., 1980. Il giacimento della Purga di Bolca (Verona), in: i vertebrati fossili italiani. Catalogo della Mostra, Verona, pp. 147–148.
Merle, R., Marzoli, A., Aka, F.T., Chiaradia, J.M., Reisberg, L., Castorina, F., Jourdan, F., Renne, P.R., N'ni, J., Nyobe, J.B., 2017. Mt. Bambouto Volcano, Cameroon Line: mantle source and differentiation of within-plate alkaline rocks. J. Petrol. 58, 933–962. https://doi.org/10.1093/petrology/egx041.
Meyzen, C.M., Marzoli, A., Bellieni, G., Levresse, G., 2016. Magmatic activity on a motionless plate: the case of East Island, Crozet Archipelago (Indian Ocean). J. Petrol.

57, 1409–1436. https://doi.org/10.1093/petrology/egw045.
Milani, L., Beccaluva, L., Coltorti, M., 1999. Petrogenesis and evolution of the Euganean magmatic complex, north eastern Italy. Eur. J. Mineral. 11, 379–399. https://doi.org/10.1127/ejm/11/2/0379.
Moine, B.N., Grégoire, M., O'Reilly, S.Y., Sheppard, S.M.F., Cottin, J.Y., 2001. High field strenght elemental fractionation in the Upper Mantle: evidence from amphibole-rich composite mantle xenoliths from the Kerguelen Islands (Indian Ocean). J. Petrol. 11, 2145–2167. https://doi.org/10.1093/petrology/42.11.2145.
Morten, L., Taylor, L.A., Durazzo, A., 1989. Spinel in harzburgite and lherzolite inclusions from the San Giovanni Ilarione Quarry, Lessini Mountains, Veneto Region, Italy. Mineral. Petrol. 40, 73–89. https://doi.org/10.1007/BF01162470.
Neumann, F., Vásquez-Serrano, A., Tolson, G., Negrete-Aranda, R., Contreras, J., 2016. Toroidal, counter-toroidal, and upwelling flow in the mantle wedge of the Rivera and Cocos plates: implications for IOB geochemistry in the Trans–Mexican Volcanic Belt. Pure Appl. Geophys. 176, 3395–3417. https://doi.org/10.1007/978–3–319–51529–8_11.
Nievergelt, P., Liniger, M., Froitzheim, N., Mählmann, R., 1996. Early to mid Tertiary crustal extension in the Central Alps: the Turba mylonite zone (eastern Switzerland). Tectonics 15, 329–340. https://doi.org/10.1029/93TC02312.
Niu, Y., 2017. Slab breakoff: a causal mechanism or pure convenience? Sci. Bull. 62, 456–461. https://doi.org/10.1016/j.scib.2017.03.015.
Niu, Y., Wilson, M., Humphreys, E.R., O'Hara, M.J., 2011. The origin of intra-plate ocean island basalts (OIB): the lid effect and its geodynamic implications. J. Petrol. 52, 1443–1468. https://doi.org/10.1093/petrology/egr030.
Oberli, F., Meier, M., Berger, A., Rosenberg, C.L., Gieré, R., 2004. U–Th–Pb and $^{230}Th/^{238}U$ disequilibrium isotope systematics: precise accessory mineral chronology and melt evolution tracing in the Alpine Bergell intrusion. Geochim. Cosmochim. Acta 68, 2543–2560. https://doi.org/10.1016/j.gca.2003.10.017.
O'Brien, P.J., 2001. Subduction followed by collision: Alpine and Himalayan examples. Phys. Earth Planet. Inter. 127, 277–291. https://doi.org/10.1016/S0031-9201(01)00232-1.
Oostingh, K.F., Jourdan, F., Matchan, E.L., Phillips, D., 2017. Ar/Ar geochronology reveals rapid change from plume-assisted to stress-dependent volcanism in the Newer Volcanic Province, SE Australia. Geochem. Geophys. 18, 1–25. https://doi.org/10.1002/2016GC006601.
Pacanovsky, K.M., Davis, D.M., Richardson, R.M., Coblentz, D.D., 1999. Intraplate stresses and plate-driving forces in the Philippine Sea plate. J. Geophys. Res. 104, 1095–1110. https://doi.org/10.1029/98JB02845.
Pallares, C., Quidelleur, X., Gillot, P.Y., Kluska, J.M., Tchilinguirian, P., Sarda, P., 2016. The temporal evolution of back-arc magmas from the Auca Mahuida shield volcano (Payenia Volcanic Province, Argentina). J. Volcanol. Geotherm. Res. 323, 19–37. https://doi.org/10.1016/j.jvolgeores.2016.04.043.
Panza, G.F., Suhadolc, P., 1990. Properties of the lithosphere in collisional belts in the Mediterranean - a review. Tectonophysics 182, 39–46. https://doi.org/10.1016/0040–1951(90)90340–E.
Papazzoni, C.A., Giusberti, L., Carnevale, G., Roghi, G., Bassi, D., Zorzin, R., 2014. The Bolca Fossil-Lagerstätten: a window into the Eocene World. Rend. Soc. Paleontol. Ital. 4.
Pedersen, T., Ro, H.E., 1992. Finite extension and decompression melting. Earth Planet. Sci. Lett. 113, 15–22. https://doi.org/10.1016/0012–821X(92)90208–D.
Pfänder, J.A., Jung, S., Klügel, A., Münker, C., Romer, R.L., Sperner, B., Rohrmüller, J., 2018. Recurrent local melting of metasomatised lithospheric mantle in response to continental rifting: constraints from basanites and nephelinites/melilitites from SE Germany. J. Petrol. 59, 667–694. https://doi.org/10.1093/petrology/egy041.
Piccoli, G., Bellati, R., Binotti, C., Di Lallo, E., Sedea, R., Dal Prà, A., Cataldi, R., Gatto, G.O., Ghezzi, G., Marchetti, N., Bulgarelli, G., Schiesaro, G., Panichi, C., Tongiorgi, E., Baldi, P., Ferrara, G.C., Massari, F., Medizza, F., Iliceto, V., Norinelli, A., De Vecchi, G., Gregnanin, A., Piccirillo, E.M., Sbettega, G., 1976. Il sistema idrotermale euganeo-berico e la geologia dei Colli Euganei. Mem. Ist. Geol. Min. Univ. Pad. 30, 266.
Piccoli, G., Sedea, R., Bellati, R., Di Lallo, E., Medizza, F., Girardi, A., De Pieri, R., Vecchi, De, Gregnanin, A., Piccirillo, E.M., Norinelli, A., Dal Prà, A., 1981. Note illustrative della carta geologica dei Colli Euganei alla scala 1: 25.000. Mem. Sci. Geol. 34, 523–546.
Piromallo, C., Faccenna, C., 2004. How deep can we find the traces of Alpine subduction? Geophys. Res. Lett. 31, L06605. https://doi.org/10.1029/2003GL019288.
Piromallo, C., Morelli, A., 2003. P wave tomography of the mantle under the Alpine-Mediterranean area. J. Geophys. Res. 108 (B2), 2065. https://doi.org/10.1029/2002JB001757.
Piromallo, C., Becker, T.W., Funiciello, F., Faccenna, C., 2006. Three-dimensional instantaneous mantle flow induced by subduction. Geophys. Res. Lett. 33, L08304. https://doi.org/10.1029/2005GL025390.
Pleuger, J., Nagel, T.J., Walter, J.M., Jansen, E., Froitzheim, N., 2008. On the role and importance of orogen -parallel and -perpendicular extension, transcurrent shearing, and backthrusting in the Monte Rosa nappe and the Southern Steep Belt of the Alps (Penninic zone, Switzerland and Italy). In: Siegesmund, S., Fügenschuh, B., Froitzheim, N. (Eds.), Tectonic Aspects of the Alpine–Dinaride–Carpathian System. Geol. Soc. Spec. Publ. London, vol. 298. pp. 251–280.
Ratschbacher, L., Frisch, W., Neubauer, F., Schmid, S.M., Neugebauer, J., 1989. Extension in compressional orogenic belts: the eastern Alps. Geology 17, 404–407. https://doi.org/10.1130/0091–7613(1989)017<0404:EICOBT>2.3.CO;2.
Ratschbacher, L., Frisch, W., Linzer, H.G., Merle, O., 1991. Lateral extrusion in the Eastern Alps, part 2: Structural analysis. Tectonics 10, 257–271. https://doi.org/10.1029/90TC02623.
Ring, U., 1994. The kinematics of the late Alpine Muretto fault and its relation to eastward extension and to displacement at the Engadine and Periadriatic lines. Eclogae Geol. Helv. 87, 811–831.
Ring, U., Gerdens, A., 2016. Kinematics of the Alpenrhein-Bodensee graben system in the Central Alps: Oligocene/Miocene transtension due to formation of the Western Alps arc. Tectonics 35, 1367–1391. https://doi.org/10.1002/2015TC004085.
Rosenbaum, G., Lister, G.S., 2005. The Western Alps from the Jurassic to Oligocene: spatio-temporal constraints and evolutionary reconstructions. Earth Sci. Rev. 69, 281–306. https://doi.org/10.1016/j.earscirev.2004.10.001.
Rosenbaum, G., Lister, G.S., Duboz, C., 2002. Relative motions of Africa, Iberia and Europe during Alpine orogeny. Tectonophysics 359, 117–129. https://doi.org/10.1016/S0040–1951(02)00442–0.
Rosenberg, C.L., 2004. Shear zones and magma ascent: a model based on a review of the Tertiary magmatism in the Alps. Tectonics 23, TC3002. https://doi.org/10.1029/2003TC001526.
Rubatto, D., Gebauer, D., Fanning, M., 1998. Jurassic formation and Eocene subduction of the Zermatt-Saas-fee ophiolites: implications for the geodynamic evolution of the Central and Western Alps. Contrib. Mineral. Petrol. 132, 269–287. https://doi.org/10.1007/s004100050421.
Savelli, C., Lipparini, E., 1979. Età K/Ar di basalti del vicentino e la scala dei tempi del Paleogene. Boll. Soc. Geol. Ital. 98, 375–385.
Schaltegger, U., Brack, P., Ovtcharova, M., Peytcheva, I., Schoene, B., Stracke, A., Marocchi, M., Bargossi, G.M., 2009. Zircon and titanite recording 1.5 million years of magma accretion, crystallization and initial cooling in a composite pluton (southern Adamello batholith, northern Italy). Earth Planet. Sci. Lett. 286, 208–218. https://doi.org/10.1016/j.epsl.2009.06.028.
Schaltegger, U., Nowak, A., Ulianov, A., Fisher, C.M., Gerdes, A., Spikings, R., Whitehouse, M.J., Bindeman, I., Hancher, J.M., Duff, J., Vervoot, J.D., Sheldrake, T., Caricchi, L., Brack, P., Müntener, O., 2019. Zircon petrochronology and $^{40}Ar/^{39}Ar$ thermocronology of the Adamello intrusive suite, N-Italy: monitoring the growth and decay of an incrementally assembled magmatic system. J. Petrol. https://doi.org/10.1093/petrology/egz010. Accepted manuscript.
Schlunegger, F., Kissling, E., 2015. Slab rollback orogeny in the Alps and evolution of the Swiss Molasse basin. Nat. Commun. 6 (8605), 1–10. https://doi.org/10.1038/ncomms9605.
Schmid, S.M., Fügenschuch, B., Kissling, E., Schuster, R., 2004. Tectonic map and overall architecture of the Alpine orogen. Eclogae Geol. Helv. 97, 93–117. https://doi.org/10.1007/s00015–004–1113–x.
Schmid, S.M., Kissiling, E., Diehl, T., van Hinsbergen, D.J.J., Molli, G., 2017. Ivrea mantle wedge, arc of the Western Alps, and kinematic evolution of the Alps-Apennines orogenic system. Swiss J. Geosci. 110, 581–612. https://doi.org/10.1007/s00015–016–0237–0.
Schmitz, M.D., Bowring, S.A., Ludwig, K.R., Renne, P.R., 2003. Comment on "Precise K–Ar, $^{40}Ar–^{39}Ar$, Rb–Sr and U–Pb mineral ages from the 27.5 fish Canyon Tuff reference standard" by M.A. Lanphere and H. Baadsgaard. Chem. Geol. 199, 277–280. https://doi.org/10.1016/S0009–2541(03)00078–0.
Schoene, B., Schaltegger, U., Brack, P., Latkoczy, C., Stracke, A., Günther, D., 2012. Rates of magma differentiation and emplacement in a ballooning pluton recorded by U–Pb TIMS–TEA, Adamello batholith, Italy. Earth Planet. Sci. Lett. 355, 162–173. https://doi.org/10.1016/j.epsl.2012.08.019.
Scott, J.M., Brenna, M., Crase, J.A., Waight, T.E., van der Meer, Q.H.A., Cooper, A.F., Palin, J.M., Le Roux, P., Münker, C., 2016. Peridotitic lithosphere metasomatized by volatile-bearing melts, and ots association with intraplate alkaline HIMU-like magmatism. J. Petrol. 57, 2053–2078. https://doi.org/10.1093/petrology/egw069.
Seghedi, I., Mațenco, L., Downes, H., Mason, P.R.D., Szakács, A., Pécskay, Z., 2011. Tectonic significance of changes in post-subduction Pliocene-Quaternary magmatism in the south east part of the Carpathian-Pannonian Region. Tectonophysics 502, 146–157. https://doi.org/10.1016/j.tecto.2009.12.003.
Siena, F., Coltorti, M., 1989. Lithospheric mantle evolution: evidences from ultramafic xenoliths in the Lessinean volcanics (Northern Itlay). Chem. Geol. 77, 347–364.
Siena, F., Coltorti, M., 1993. Thermobarometric evolution and metasomatic processes of upper mantle in different tectonic settings: evidence from spinel peridotite xenoliths. Eur. J. Mineral. 5, 1073–1090.
Singer, J., Diehl, T., Hunsen, S., Kissiling, E., Duretz, T., 2014. Alpine lithophere slab rollback causing lower crustal seismicity in northern foreland. Earth Planet. Sci. Lett. 397, 42–56. https://doi.org/10.1016/j.epsl.2014.04.002.
Sokol, A.G., Kruk, A.N., Palyanov, Y.N., Sobolev, N.V., 2017. Stability of phlogopite in ultrapotassic kimberlite-like systems at 5.5–7.5 GPa. Contrib. Mineral. Petrol. 172, 21. https://doi.org/10.1007/s00410–017–1341–5.
Sorbini, L., 1989. I Fossili Di Bolca. Museo Civico di Storia Naturale di Verona, Verona.
Stampfli, G.M., Mosar, J., Marquer, D., Marchant, R., Baudin, T., Borel, G., 1998. Subduction and obduction processes in the Swiss Alps. Tectonophysics 296, 159–204. https://doi.org/10.1016/S0040–1951(98)00142–5.
Stampfli, G.M., Borel, G.D., Marchant, R., Mosar, J., 2002. Western Alps geological constraints on western Tethyan reconstruction. In: Rosenbaum, G., Lister, G.S. (Eds.), Reconstruction of the evolution of the Alpine-Himalayan Orogen. J. Virt. Expl. 7. pp. 75–104.
Steck, A., 2008. Tectonics of the Simplon massif and Lepontine gneiss dome: Deformation structures due to collision between the underthrusting European plate and the Adriatic indenter. Swiss J. Geosci. 101, 515–546. https://doi.org/10.1007/s00015–008–1283–z.
Strak, V., Schellart, W.P., 2014. Evolution of 3–D subduction–induced mantle flow around lateral slab edges in analogue models of free subduction analysed by stereoscopic particle image velocimetry technique. Earth Planet. Sci. Lett. 403, 368–379. https://doi.org/10.1016/j.epsl.2014.07.007.
Su, B.-X., Zhang, H.-F., Sakyi, P.A., Ying, J.-F., Tang, Y.-J., Yang, Y.-H., Qin, K.-Z., Xiao, Y., Zhao, X.-M., 2010. Compositionally stratified lithosphere and carbonatite metasomatism recorded in mantle xenoliths from Western Qinling (Central China). Lithos 116, 111–128. https://doi.org/10.1016/j.lithos.2010.01.004.

Sun, S.S., McDonough, W.F., 1989. Chemical and isotopic systematics of oceanic basalts: Implications for mantle composition and processes. In: Saunders, A.D., Norry, M.J. (Eds.), Magmatism in the Oceanic Basins. Geol. Soc. Spec. Publ. London, vol. 42. pp. 313–346.

Tang, Y., Obayashi, M., Niu, F., Grand, S.P., Chen, Y.J., Kawakatsu, H., Tanaka, S., Ning, J., Ni, J.F., 2014. Changbaishan volcanism in Northeast China linked to subduction-induced mantle upwelling. Nat. Geosci. 7, 470–475. https://doi.org/10.1038/ngeo2166.

Thirlwall, M.F., Upton, B.G.J., Jenkins, C., 1994. Interaction between continental lithosphere and the Iceland plume.Sr–Nd–Pb isotope chemistry of Tertiary basalts, NE Greenland. J. Petrol. 35, 839–897. https://doi.org/10.1093/petrology/35.3.839.

Tiepolo, M., Oberti, R., Zanetti, A., Vannucci, R., Foley, S.F., 2007. Trace-element partitioning between amphibole and silicate melt. Rev. Mineral. Geochem. 67, 417–452. https://doi.org/10.2138/rmg.2007.67.11.

van Westrenen, W., Blundy, J.D., Wood, B.J., 2001. High field strength element/rare element fractionation during partial melting in the presence of garnet: implications for identification of mantle heterogeneities. Geochem. Geophys. https://doi.org/10.1029/2000GC000133. 2000GC000133.

Verati, C., Jourdan, F., 2013. Modelling effect of sericitization of plagioclase on the $^{40}K/^{40}Ar$ and $^{40}K/^{39}Ar$ chronometers: Implication for dating basaltic rocks and mineral deposits. In: Jourdan, F., Mark, D.F., Verati, C. (Eds.), Advances in $^{40}Ar/^{39}Ar$ Dating: From Archaeology to Planetary Sciences. Geol. Soc. Spec. Publ. London, vol. 378. pp. 155–174. https://doi.org/10.1144/SP378.24.

Verma, S.P., 2002. Absence of Cocos plate subduction related basic volcanism in southern Mexico: a unique case on Earth? Geology 30, 1095–1098. https://doi.org/10.1130/0091–7613(2002)030<1095:AOCPSR>2.0.CO;2.

Visonà, D., Caironi, V., Carraro, A., Dallai, L., Fioretti, A.M., Fanning, M., 2007. Zircon megacrysts from basalts of the venetian Volcanic Province (NE Italy): U–Pb, oxygen isotopes and REE data. Lithos 94, 168–180. https://doi.org/10.1016/j.lithos.2006.06.007.

von Blanckenburg, F., 1992. Combined high-precision chronometry and geochemical tracing using accessory minerals: applied to the Central-Alpine Bergell intrusion (Central Europe). Chem. Geol. 100, 19–40. https://doi.org/10.1016/0009-2541(92)90100-J.

von Blanckenburg, F., Davies, J.H., 1995. Slab breakoff: a model for syncollisional magmatism and tectonics in the Alps. Tectonics 14, 120–131. https://doi.org/10.1029/94TC02051.

Wedepohl, K.H., Baumann, A., 1999. Central European Cenozoic plume volcanism with OIB characteristics and indications of a lower mantle source. Contrib. Mineral. Petrol. 136, 225–239. https://doi.org/10.1007/s004100050534.

Wilson, M., Downes, H., 1991. Tertiary-Quaternary extension-related alkaline magmatism in western and Central Europe. J. Petrol. 32, 811–849. https://doi.org/10.1093/petrology/32.4.811.

Wilson, M., Downes, H., 1992. Mafic alkaline magmatism in the European Cenozoic rift system. Tectonophysics 208, 173–182. https://doi.org/10.1016/0040-1951(92)90343-5.

Wilson, M., Downes, H., 2006. Tertiary-Quaternary intra-plate magmatism in Europe and its relationship to mantle dynamics. In: Gee, D., Stephenson, R. (Eds.), European Lithosphere Dynamics. Geol. Soc. Lond. Mem, vol. 32. pp. 147–166. https://doi.org/10.1144/GSL.MEM.2006.032.01.09.

Wilson, M., Patterson, R., 2001. Intraplate magmatism related to shortwavelength convective instabilities in the upper mantle: evidence from the Tertiary-Quaternary volcanic province of western and Central Europe. In: Ernst, R.E., Buchan, K.L. (Eds.), Mantle Plumes: Their Identification Through Time. Geol. Soc. Am. Spec. Paper, vol. 352. pp. 37–58. https://doi.org/10.1130/0-8137-2352-3.37.

Winterer, E.L., Bosellini, A., 1981. Subsidence and sedimentation on a Jurassic passive continental margin (Southern Alps, Italy). Bull. Am. Assoc. Pet. Geol. 65, 394–421.

Wörner, G., Zindler, A., Staudigel, H., Schmincke, H.U., 1986. Sr, Nd and Pb isotope geochemistry of Tertiary and Quaternary volcanics from West Germany. Earth Planet. Sci. Lett. 79, 107–119. https://doi.org/10.1016/0012-821X(86)90044-0.

Yang, Q.Y., Santosh, M., 2014. Early cretaceous magma flare-up and its implications on gold mineralization in the Jiaodong Peninsula. China. Ore Geol. Rev. 65, 626–642. https://doi.org/10.1016/j.oregeorev.2014.01.004.

Yaxley, G.M., Crawford, A.J., Green, D.H., 1991. Evidence for carbonatite metasomatism in spinel peridotite xenoliths from western Victoria, Australia. Earth Planet. Sci. Lett. 107, 305–317. https://doi.org/10.1016/0012–821X(91)90078–V.

Zampieri, D., 1995. Tertiary extension in the southern Trento Platform, Southern Alps, Italy. Tectonics 14, 645–657. https://doi.org/10.1029/94TC03093.

Zanazzi, P.F., Pavese, A., 2002. Behavior of micas at high pressure and high temperature. Rev. Mineral. Geochem. 46, 98–116. https://doi.org/10.2138/rmg.2002.46.02.

Zanetti, A., Mazzucchelli, M., Rivalenti, G., Vannucci, R., 1999. The Finero-phlogopite peridotite massif: an example of subduction-related metasomatism. Contrib. Mineral. Petrol. 134, 107–122. https://doi.org/10.1007/s004100050472.

Zantendeschi, C., 1994. New Rb–Sr radiometric data from Colli Euganei (North Eastern Italy). Mem. Ist. Geol. Min. Univ. Pad. 46, 17–22.

Zhao, L., Paul, A., Malusà, M.G., Xiaobing, X., Zheng, T., Solarino, S., Guillot, S., Schwartz, S., Dumont, T., Salimbeni, S., Aubert, A., Pondrelli, S., Wang, Q., Zhu, R., 2016. Continuity of the Alpine slab unraveled by high-resolution P wave tomography. J. Geophys. Res. Solid Earth 121, 8720–8737. https://doi.org/10.1002/2016JB013310.

Ziberna, L., Klemme, S., Nimis, P., 2013. Garnet and spinel in fertile and depleted mantle: insights from thermodynamic modelling. Contrib. Mineral. Petrol. 166, 411–421. https://doi.org/10.1007/s00410–013–0882–5.